



Year: 2018

Effect of environmental conditions on sun-induced fluorescence in a mixed forest and a cropland

Paul-Limoges, Eugénie ; Damm, Alexander ; Hueni, Andreas ; Liebisch, Frank ; Eugster, Werner ; Schaeepman, Michael E ; Buchmann, Nina

Abstract: Due to the large carbon dioxide (CO₂) fluxes between terrestrial ecosystems and the atmosphere, dynamics of photosynthesis can have significant effects on atmospheric CO₂ concentrations and lead to large uncertainties in ecosystem C budgets. Remote sensing approaches using sun-induced chlorophyll fluorescence (SIF) hold the potential to directly assess ecosystem photosynthesis. However, many challenges remain linked to using the SIF emission signal to estimate gross primary production (GPP). The goal of this study was to gain a better understanding of the relationships between GPP and SIF over different time scales (minutes to years) and under varying environmental conditions. Two different ecosystems were investigated, a cropland and a mixed forest, with continuous eddy covariance flux measurements. Continuous tower-based SIF retrievals were performed in 2015 and 2016 at both ecosystems. In both ecosystems, SIF was found to be more affected by environmental conditions than GPP. Annual cycles for GPP and SIF differed at the mixed forest due in part to the influence of the different footprint size of the two independent measurements. Diurnal cycles in GPP and SIF corresponded well under unstressed conditions and followed the incoming photosynthetic photon flux density (PPFD). However, depressions in SIF were found at both sites either at midday or in the afternoon during the growing season. At the cropland site, reductions in SIF occurred at high PPFD (PPFD > 1470 μmol m⁻² s⁻¹, R² = 0.62) and high VPD (VPD > 1590 Pa, R² = 0.35). Whereas at the forest site, reductions in SIF were linked to high VPD (VPD > 1250 Pa, R² = 0.25), but not to high PPFD (R² = 0.84). The depression in SIF was also associated with an increase in non-photochemical quenching, as indicated by the photochemical reflectance index (R² = 0.78), thus showing the complementarity between SIF and non-photochemical quenching as different energy pathways. Our results show the importance of characterizing the influence of different environmental conditions on SIF-GPP relationships for specific ecosystems to reliably estimate GPP from remote sensing measurements.

DOI: <https://doi.org/10.1016/j.rse.2018.10.018>

Posted at the Zurich Open Repository and Archive, University of Zurich

ZORA URL: <https://doi.org/10.5167/uzh-161329>

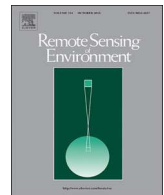
Journal Article

Published Version

Originally published at:

Paul-Limoges, Eugénie; Damm, Alexander; Hueni, Andreas; Liebisch, Frank; Eugster, Werner; Schaeepman, Michael E; Buchmann, Nina (2018). Effect of environmental conditions on sun-induced fluorescence in a mixed forest and a cropland. *Remote Sensing of Environment*, 219:310-323.

DOI: <https://doi.org/10.1016/j.rse.2018.10.018>



Effect of environmental conditions on sun-induced fluorescence in a mixed forest and a cropland

Eugénie Paul-Limoges^{a,b,*}, Alexander Damm^{b,c}, Andreas Hueni^b, Frank Liebisch^a, Werner Eugster^a, Michael E. Schaepman^b, Nina Buchmann^a

^a Institute of Agricultural Sciences, ETH Zurich, Universitätstrasse 2, 8092 Zurich, Switzerland

^b Department of Geography, University of Zurich, Winterthurerstrasse 190, 8057 Zurich, Switzerland

^c Department of Surface Waters – Research and Management, Eawag, Swiss Federal Institute of Aquatic Science and Technology, 8600 Dübendorf, Switzerland



ARTICLE INFO

Keywords:

Gross primary production
Midday depression
Photoinhibition
Diurnal cycles
Water stress
Vapour pressure deficit

ABSTRACT

Due to the large carbon dioxide (CO_2) fluxes between terrestrial ecosystems and the atmosphere, dynamics of photosynthesis can have significant effects on atmospheric CO_2 concentrations and lead to large uncertainties in ecosystem C budgets. Remote sensing approaches using sun-induced chlorophyll fluorescence (SIF) hold the potential to directly assess ecosystem photosynthesis. However, many challenges remain linked to using the SIF emission signal to estimate gross primary production (GPP). The goal of this study was to gain a better understanding of the relationships between GPP and SIF over different time scales (minutes to years) and under varying environmental conditions. Two different ecosystems were investigated, a cropland and a mixed forest, with continuous eddy covariance flux measurements. Continuous tower-based SIF retrievals were performed in 2015 and 2016 at both ecosystems.

In both ecosystems, SIF was found to be more affected by environmental conditions than GPP. Annual cycles for GPP and SIF differed at the mixed forest due in part to the influence of the different footprint size of the two independent measurements. Diurnal cycles in GPP and SIF corresponded well under unstressed conditions and followed the incoming photosynthetic photon flux density (PPFD). However, depressions in SIF were found at both sites either at midday or in the afternoon during the growing season. At the cropland site, reductions in SIF occurred at high PPFD ($\text{PPFD} > 1470 \mu\text{mol m}^{-2} \text{s}^{-1}$, $R^2 = 0.62$) and high VPD (VPD $> 1590 \text{ Pa}$, $R^2 = 0.35$). Whereas at the forest site, reductions in SIF were linked to high VPD (VPD $> 1250 \text{ Pa}$, $R^2 = 0.25$), but not to high PPFD ($R^2 = 0.84$). The depression in SIF was also associated with an increase in non-photochemical quenching, as indicated by the photochemical reflectance index ($R^2 = 0.78$), thus showing the complementarity between SIF and non-photochemical quenching as different energy pathways. Our results show the importance of characterizing the influence of different environmental conditions on SIF-GPP relationships for specific ecosystems to reliably estimate GPP from remote sensing measurements.

1. Introduction

Terrestrial gross primary production (GPP) is the largest global CO_2 flux, estimated at 120 Pg C yr^{-1} (e.g. Ballantyne et al., 2017; Beer et al., 2010), and absorbs approximately one third of anthropogenic CO_2 emissions (Le Quéré et al., 2015). Dynamics of photosynthesis can therefore have important effects on atmospheric CO_2 concentrations and lead to large uncertainties in ecosystem C budgets. There is currently debate as to whether this vegetation sink will continue to buffer the effects of increased CO_2 emissions in a changing climate (Friedlingstein et al., 2006; Knorr, 2009; Le Quéré et al., 2012; Sitch

et al., 2008). Many challenges are however faced when observing the highly dynamic process of photosynthesis at ecologically relevant scales, as it is controlled by many biological and environmental factors acting at different temporal (Rascher and Nedbal, 2006; Schurr et al., 2006) and spatial (Nemani et al., 2003) scales. Reliable monitoring systems are thus required to increase the knowledge on spatial and temporal dynamics of plant photosynthesis and associated ecosystem C sequestration rates.

At ecosystem level, eddy-covariance (EC) measurements give a detailed and continuous temporal record of the CO_2 fluxes at many locations worldwide through FLUXNET (Baldocchi et al., 2001).

* Corresponding author at: Institute of Agricultural Sciences, ETH Zurich, Universitätstrasse 2, 8092 Zurich, Switzerland.
E-mail address: eugenie.paul-limoges@geog.uzh.ch (E. Paul-Limoges).

However, the spatial scale of the measurements (typically a few 100 m² in croplands to 1 km² or more in forests) has limitations when it comes to covering larger areas globally and generalizing to entire ecoregions (see e.g. Paul-Limoges et al., 2015) due to the spatial variability. EC measurements often represent only small areas in selected ecosystems (Drolet et al., 2008; Turner et al., 2005; Turner et al., 2003). On the other hand, remote sensing offers the possibility to investigate C uptake over larger areas, but often lacks accuracy due to the generality of the proxies used, e.g. vegetation indices, and to the lack of ground validations.

Previous studies have demonstrated that remote sensing indices based on canopy cover and greenness (e.g. NDVI, EVI) are not sensitive enough to capture short-term variations and seasonal dynamics of vegetation, especially for evergreen canopies (Dobrowski et al., 2005; Garbulsky et al., 2014; Walther et al., 2016; Zarco-Tejada et al., 2013). In contrast, physiological indices are more sensitive to vegetation dynamics and to small physiological changes occurring in canopies, thus allowing for a more accurate representation of the actual photosynthesis than canopy cover and greenness based indices (Dobrowski et al., 2005; Gamon et al., 2016; Garbulsky et al., 2014; Zarco-Tejada et al., 2013). New and emerging remote sensing approaches allow to measure sun-induced chlorophyll fluorescence (SIF), a physiological index, and hold the potential to directly assess ecosystem photosynthesis and related C sequestration (e.g. Beer et al., 2010; Damm et al., 2010; Flexas et al., 2000; Flexas et al., 2002; Porcar-Castell et al., 2014). Significant developments have been achieved over the last decade in measuring SIF, thereby opening a new opportunity to assess actual photosynthesis and GPP (e.g. Damm et al., 2015a; Guanter et al., 2014). However, many challenges remain linked to understanding the chlorophyll fluorescence signal in order to obtain accurate GPP estimates.

One of the main limitations linked to remotely sensed SIF is the scarce knowledge of how it relates to vegetation functioning (Garbulsky et al., 2014). While some studies have demonstrated that satellite-derived SIF is linearly related to GPP at a global scale (Guanter et al., 2014), this linearity at the global scale is likely linked to the temporal and spatial averaging and is therefore not representative at plant or ecosystem scales (Damm et al., 2015a). As SIF is directly linked to the photosynthetic activity in photosystem II (PS II), it is strongly affected by environmental conditions causing stress for plants (e.g. Ać et al., 2015). Different moisture or light conditions are most likely to affect the mechanistic relationships found under more ideal conditions, although it is still unknown in which way. Furthermore, two pathways compete to de-excite the absorbed light energy that is not used in photochemistry: the energy can be emitted as SIF or dissipated as heat through NPQ (Porcar-Castell et al., 2014). The proportion of energy allocated to each pathway will vary under different environmental conditions (Flexas and Medrano, 2002; Maxwell and Johnson, 2000), possibly affecting the SIF-GPP relationships. In addition, as airborne and spaceborne remote sensing requires a cloudless sky for accurate measurements, there is a strong bias associated with under-sampling under diffuse light conditions (Mercado et al., 2009; Parazoo et al., 2014). Thus, it is currently unknown how more diffuse light conditions affect SIF. Further studies are therefore needed to quantify mechanistic relationships between SIF and GPP under different environmental conditions (Lee et al., 2013; Maxwell and Johnson, 2000).

As airborne and spaceborne remote sensing usually provide only a snapshot of SIF in time, it is difficult to assess the influence of temporal dynamics and effect of environmental conditions on SIF due to the lack of a temporally continuous signal. A recent study by Verma et al. (2017) assessed the effect of environmental conditions on SIF-GPP relationships, using SIF data from the Orbiting Carbon Observatory-2 (OCO-2). They observed strong linear relationships between SIF and GPP, based on 14 observations over two years. Although they were able to capture different environmental conditions, these are still very few measurements compared to the variability that occurs in GPP and SIF in ecosystems, even on a daily basis. Similarly, Wood et al. (2017) and Sun

et al. (2017) found a linear relationship between SIF from OCO-2 and GPP from flux tower measurements, with no sign of light saturation, based on SIF measurements occurring always at the same time (for e.g. 13:30 local time) at their sites. In comparison, Li et al. (2018) found asymptotic relationships between OCO-2 SIF and GPP in temperate forests. In addition, they found that SIF was also affected by environmental stresses that affect the photosynthetic light use efficiency (e.g. VPD and temperature), in a similar way as GPP.

The overarching goal of our study was to investigate the relationship between GPP and SIF using ecosystem-based temporally-continuous data under different environmental conditions. The objectives of this study were to (1) derive a continuous temporal SIF signal from tower-based spectrometers to compare to GPP estimates from EC flux measurements, (2) investigate annual and diurnal variations in SIF at two different ecosystems — a cropland and a mixed forest, and (3) assess the influence of different environmental conditions on SIF emissions and on the resulting functional relationships with GPP.

2. Methods

2.1. Research sites

Two sites located on the Central Swiss Plateau were investigated. The two sites Oensingen and Lägeren are part of Swiss FluxNet since 2004, and are thus equipped with EC flux towers and meteorological stations. These two sites differ in their structure, heterogeneity, species composition and productivity. The Oensingen cropland site (47°17'11.1" N, 7°44'01.5" E, 452 m a.s.l.), located near the town of Oensingen, is an agricultural field, with the dominant crops during the study years being winter barley (*Hordeum vulgare* L.), followed by cover crop after harvest (2015), and pea (*Pisum sativum*) (2016). The growing seasons at Oensingen were from March until end of June in 2015, and from April until end of July in 2016. The Lägeren forest site (47°28'42.0" N, 8°21'51.8" E, 682 m a.s.l.) is located on the south-facing slope of the Lägeren mountain ridge, northwest of the city of Zurich. The temperate mixed forest is characterized by a relatively high species diversity and a complex canopy structure, with European beech (*Fagus sylvatica* L.), ash (*Fraxinus excelsior* L.), European silver fir (*Abies alba* Mill.), sycamore maple (*Acer pseudoplatanus*), and Norway spruce (*Picea abies* (L.) Karst.) as the dominant species (Eugster et al., 2007). The mean tree height is 30.6 m (Etzold et al., 2011), and the mean leaf area index (LAI) during the vegetation period ranges from 1.7 to 5.5 m² m⁻². The growing season at the Lägeren site is from May until end of August. The understory is dominated by wild garlic (*Allium ursinum*) during spring and early summer as well as seedlings and saplings.

2.2. Environmental measurements

Climate variables were measured at a height of 2 m at the Oensingen site and at a height of 47 m at the Lägeren site. Air temperature (T_a) and relative humidity (RH) were measured using a combined temperature and relative humidity probe (Rotronic MP101A, Bassersdorf, Switzerland). The incoming direct and diffuse photosynthetic photon flux density (PPFD) was measured using a sunshine sensor (BF5 at Oensingen and BF2 at Lägeren, Delta-T Devices, Cambridge, UK). Total precipitation was measured using a heated rain gauge (Lambrecht GmbH 15188, Goettingen, Germany). Soil temperature (T_s) and volumetric water content (θ) were measured at depths of 5, 10, 20, and 30 cm using Decagon ECH₂O EC-20 probes (Pullman, WA, USA). Measurements were made every 30 s and output averaged every 30 min with a data logger (CR1000, Campbell Scientific Inc., Loughborough, UK).

2.3. Tower-based hyperspectral measurements

High precision spectrometers (UniSpec-DC, PP Systems International Inc., Amesbury, MA, USA) were installed at the Oensingen cropland site in

November 2014 and at the Lägeren forest site in January 2015. The UniSpec-DC has 256 contiguous bands with, nominally, a sampling interval of 3.1 nm, and a range of operation between 305 and 1135 nm. The UniSpec-DC features two channels to measure both solar irradiance (E) and surface reflected radiance (L) simultaneously. The spectrometers were modified to allow direct and continuous serial communication with an external data acquisition computer. The spectrometers were housed in a temperature controlled box to ensure that the temperature of the instrument varied by no more than 1 or 2 °C. The data acquisition was coded in Python (Python Software Foundation) on a Raspberry Pi (Raspberry Pi Foundation, UK) embedded Linux computer. The fiber optics from the UniSpec-DC were mounted at a height of 45 m above ground at the Lägeren site and at a height of 2 m above ground at the Oensingen site, pointing south of the tower to avoid any directional influence or shading from the tower. The footprint of the UniSpec-DC was approximately 10 m² at the Lägeren site and approximately 1 m² at the Oensingen site. The footprint of the UniSpec-DC at the Lägeren site included only deciduous trees and not any evergreen trees. Measurements of upwelling radiance and downwelling irradiance were taken every 5 min at both sites, and then averaged to half-hourly values. In January 2016, the data acquisition code was improved to deal with varying light conditions by dynamically setting optimized integration times following Pacheco-Labrador and Martin (2014), instead of the previously constant integration time that occasionally led to lack of sensitivity at low light levels, and oversaturation at high light levels. The UniSpec-DC spectrometers were radiometrically cross-calibrated to a field spectroradiometer (FieldSpec FS3, ASD Inc., Boulder, CO, USA) acting as a transfer radiometer, by measuring the same white reference panel (Spectralon, Labsphere, USA) over full days with different light intensities and direct/diffuse ratios.

SIF at 760 nm (SIF_{760}) was retrieved from tower based radiance measurements around the O₂-A absorption using the three Fraunhofer Line Depth (3FLD) approach as described in Damm et al. (2014). The retrieval method decouples fluorescence from the reflected radiance using two radiance measurements L_i inside (i , 760 nm) and L_o outside (o) of the O₂-A band. They can be expressed as:

$$L_j = L_j^p + \frac{\left(E_j^g \frac{\rho_j}{\pi} + SIF_j \right) \tau \uparrow_j}{1 - S_j * \rho_j}, j = i, o, \quad (1)$$

L^p is the path scattered radiance, E^g is the global irradiance (including direct and diffuse irradiance components) arriving on the surface, ρ is the surface reflectance, $\tau \uparrow$ is the upwelling transmittance, and S is the spherical albedo. E^g was directly measured with the upward looking channel. We assumed $L^p = 0$ and $\tau \uparrow = 1$, justified by the short distance between surface and sensor (< 10 m). Further, S was set to zero since the product of S and ρ can be assumed as ≪ 1. The remaining four unknowns of the system of equations (Eq. (1)) (i.e. ρ_i , ρ_o , SIF_i , SIF_o) had to be reduced to only two to eventually retrieve SIF. We applied the 3FLD approach originally introduced by Maier et al. (2003) to linearly relate ρ and SIF inside and outside of the O₂-A band. With this, SIF_{760} can be retrieved as:

$$SIF_{760} = SIF_i = B \left[\frac{X_i(E_i^* + X_o * S_o) - AX_o(E_i^* + X_i * S_i)}{B(E_o^* + X_o * S_o) - A(E_i^* + X_i * S_i)} \right], \quad (2)$$

with

$$X_j = \frac{(L_j - L_j^p)}{\tau \uparrow_j}, \quad E_j^* = \frac{E_j^g}{\pi} \quad j = i, o, \quad (3)$$

and

$$\rho_i = A\rho_o \quad (4)$$

$$F_i = BF_o \quad (5)$$

X_j equals the top-of-canopy (ToC) radiance leaving the surface. B is a factor relating SIF inside and outside the O₂-A band and was fixed to a value of 1.0, justified by simulations and experiments. A is the factor

relating ρ_i and ρ_o and was derived from the weighted (ω) linear interpolation of ρ using the left (average 730–745 nm, ρ_{737}) and right (average of 764–780 nm, ρ_{772}) O₂-A band shoulders with:

$$A = \frac{\rho_{737}\omega_1 + \rho_{772}\omega_2}{\rho_{737}}, \quad (6)$$

$$\omega_1 = \frac{772 - 760}{772 - 737}, \text{ and } \omega_2 = \frac{760 - 737}{772 - 737}. \quad (7)$$

Leaves emit fluorescence isotropically and hence, marginal directional effects were assumed to be measured in SIF (Culver and Perry, 1997; Moya et al., 2004; Sanders et al., 2016). Previous studies have quantified that anisotropy effects for the SIF retrieval from a setup like the ones at Lägeren and at Oensingen should be on the order of about 2% (Damm et al., 2015b; van der Tol et al., 2009b).

The photochemical reflectance index (PRI) (Gamon et al., 1992) was calculated as a proxy for non-photochemical quenching (NPQ) activity. PRI was calculated as:

$$PRI = \frac{R_{570} - R_{531}}{R_{570} + R_{531}} \quad (8)$$

where R_{570} is the reflectance at 570 nm and R_{531} is the reflectance at 531 nm. Changes in reflectance centered at 531 nm have been associated with chloroplast shrinkage and with an accumulation of de-epoxidized forms of the xanthophyll cycle molecules due to NPQ (Evain et al., 2004; Morales et al., 1990; Ruban et al., 1993), while the reflectance at 570 nm is used as a reference. A PRI fraction was calculated as the fraction of the total energy used for the two alternative pathways to photosynthesis (i.e., SIF and NPQ) used for NPQ as follow:

$$PRI_{fraction} = \frac{PRI}{SIF + PRI} \quad (9)$$

2.4. Eddy-covariance flux measurements

Turbulent fluxes of CO₂ were measured continuously at the Oensingen cropland and the Lägeren mixed forest sites in 2015 and 2016 using the eddy-covariance (EC) technique (Balocchi, 2003). The EC system at the Oensingen site was installed at a height of 2 m (Dietiker et al., 2010). The above canopy EC system at the Lägeren site was mounted at a height of 47 m (Etzold et al., 2011), and an additional below canopy EC system was measuring at a height of 1.5 m above the soil surface (Paul-Limoges et al., 2017). The EC instrumentation at each site consisted of an open-path infrared gas analyzer (IRGA) (LI-7500, LI-COR Inc., Lincoln, NE, USA) and a three-dimensional ultrasonic anemometer-thermometer (HS-100 (Lägeren above canopy) and R3-50 (Oensingen and Lägeren below canopy), Gill Instruments Ltd., Lymington, UK). The contribution of the deciduous trees at the Lägeren site was estimated by removing the contribution from the understory vegetation as measured with the below canopy EC system and by estimating the contribution from the evergreen trees based on the photosynthesis rates in winter, as the deciduous trees were not very active during the winter period (i.e., leafless). However, this estimation of the photosynthetic rate of the evergreen trees based on the winter rates likely leads to an underestimation during summer, due to the down-regulation of photosynthesis occurring in winter (Oquist and Huner, 2003). EC measurements were outputted at a frequency of 20 Hz and processed to half-hourly averages using the *EddyPro* software (v6.1.0, LI-COR Inc., USA). The statistical quality of the raw time series was assessed before flux calculations following Vickers and Mahrt (1997). Raw high-frequency data were rejected if (1) spikes accounted for more than 1% of the time series, (2) more than 10% of available data points were statistically different from the overall trend in the half-hour period, (3) raw data values were outside a plausible range, or (4) window dirtiness of the IRGA sensor exceeded 80%. Only raw data that passed all quality tests were used for flux calculations. Half-hourly

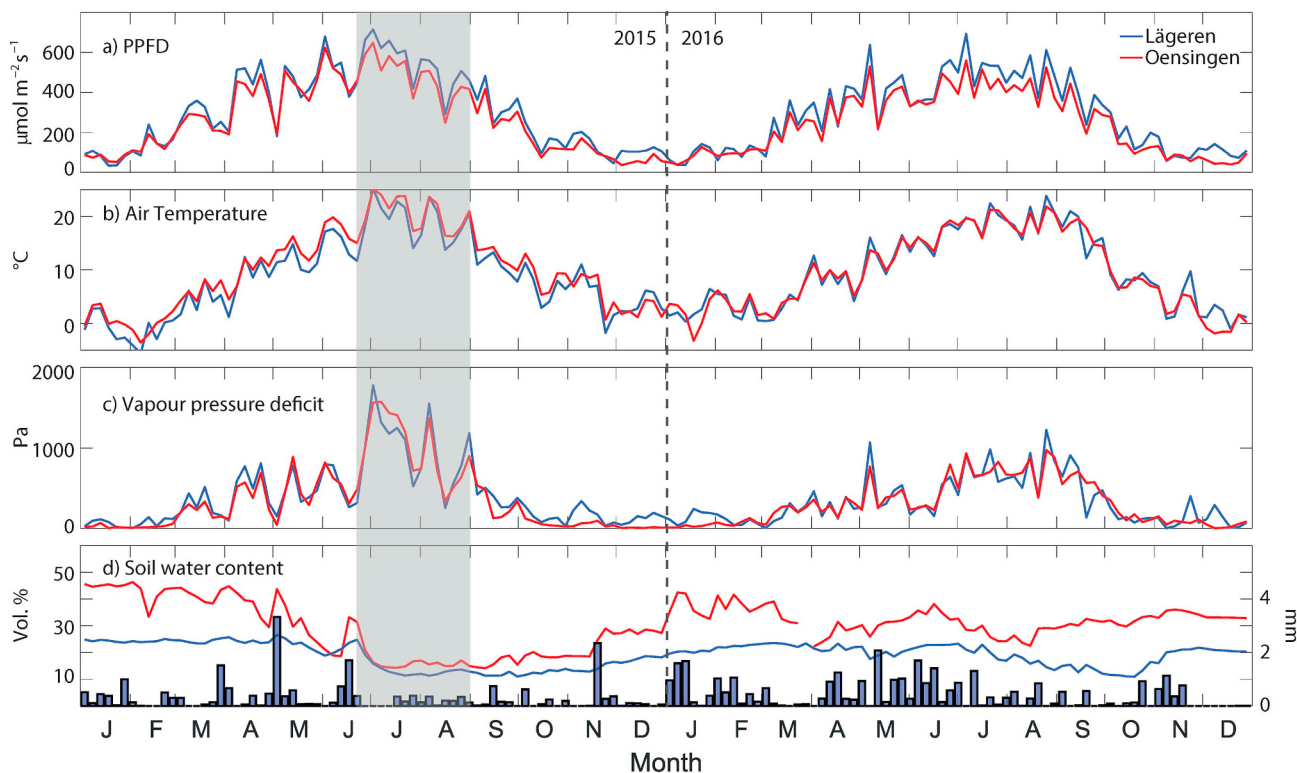


Fig. 1. Climate variables in 2015 and 2016 at Lägeren (blue line) and Oensingen (red line). The photosynthetic photon flux density (PPFD, panel a), air temperature (panel b) and vapour pressure deficit (VPD, panel c) are measured at a height of 47 m at Lägeren and at a height of 2 m at Oensingen. Soil water content (panel d) is measured at a depth of 5 cm at both sites. The blue bars in panel d represent precipitation. All lines represent 5-day averages. The gray band indicates the pronounced heat wave in 2015. (For interpretation of the references to color in this figure legend, the reader is referred to the web version of this article.)

Table 1

Equations for the relationships between SIF and PPF and for the relationships between SIF and VPD in Fig. 7.

Equations	
a) Oensingen SIF vs. PPF	$SIF = -1.2 \times 10^{-12} PPF^4 + 3.6 \times 10^{-9} PPF^3 - 3.3 \times 10^{-6} PPF^2 + 0.002 PPF - 0.02$
b) Lägeren SIF vs. PPF	$SIF = 0.0077 \exp^{0.0022 PPF}$
c) Oensingen SIF vs. VPD	$SIF = -1.5 \times 10^{-14} VPD^4 + 1.1 \times 10^{-10} VPD^3 - 4.3 \times 10^{-7} VPD^2 + 7.4 \times 10^{-4} VPD - 0.21$
d) Lägeren SIF vs. VPD	$SIF = -3.9 \times 10^{-17} VPD^5 + 3.1 \times 10^{-13} VPD^4 - 8.8 \times 10^{-10} VPD^3 + 9.7 \times 10^{-7} VPD^2 - 2.8 \times 10^{-4} VPD - 0.075$

Table 2

Equations for the relationships between SIF and the ratio of diffuse to direct PPF in Fig. 8.

Equations	
a) Oensingen SIF vs. diffuse ratio	$SIF = 1.37 \exp^{-8.4 \text{ Diffuse ratio}} + 0.67 \exp^{-1.7 \text{ Diffuse ratio}}$
b) Lägeren SIF vs. diffuse ratio	$SIF = 309.7 \exp^{-57.5 \text{ Diffuse ratio}} + 0.40 \exp^{-2.0 \text{ Diffuse ratio}}$

averaged fluxes were rejected if (1) CO₂ fluxes were outside a physically plausible range (-50 to $+50 \mu\text{mol m}^{-2} \text{s}^{-1}$), (2) the steady-state test statistic was outside the range $\pm 30\%$ (Foken et al., 2005), or (3) the integral turbulence characteristic test was outside the $\pm 30\%$ range (Foken et al., 2005). Standardized gap filling and partitioning of CO₂ fluxes into gross primary production (GPP) and ecosystem respiration was performed using the methodology from Barr et al. (2004).

3. Results

3.1. Environmental conditions in 2015 and 2016

The growing season in 2015 was drier and warmer than in 2016, due to a prolonged heat wave (Fig. 1). From May to October, average

air temperatures in 2015 (15°C) were 2°C warmer than in 2016 (13°C), while total precipitation was lower in 2015 (642 mm) compared to 2016 (891 mm). During summer (JJA), only about half (53%) the precipitation fell in 2015 (243 mm) compared to 2016 (457 mm). The heat wave in 2015 resulted in drastic reductions in soil water content, down to 10% at the Lägeren site and to 16% at the Oensingen site, a decrease of 60 to 64% at both sites (Fig. 1d). The Lägeren and Oensingen sites are separated by a distance of only 60 km and therefore, the climate experienced at both sites is quite similar (Fig. 1). However, important differences between the two sites are the vegetation cover, soil type, topography and ground water depth, which then influence climate variables that affect plant growth and vitality such as soil water content. Supplementary Fig. S 1 shows that at the Oensingen site, soil water content stayed higher at 30 and 50 cm depth, but the roots of the

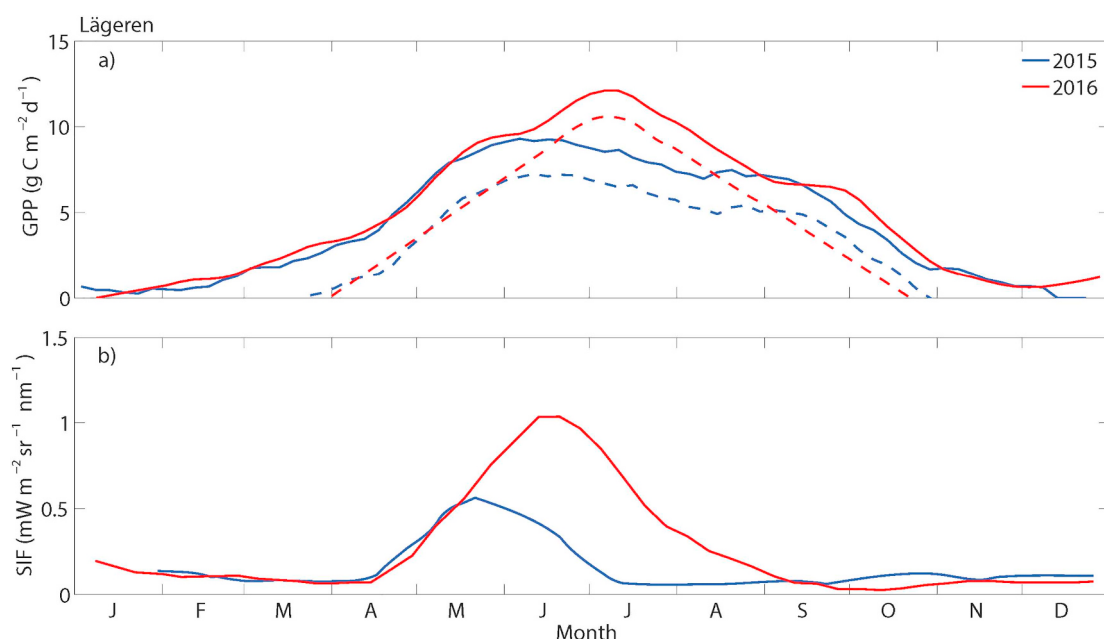


Fig. 2. Gross primary production (GPP, panel a) and sun-induced fluorescence (SIF, panel b) at the Lägeren mixed forest site in 2015 (blue line) and 2016 (red line). The dashed blue and red lines in panel a) show the estimated GPP contribution from the deciduous trees (all species) at the site, and the remaining contribution is from the understorey vegetation and evergreen coniferous trees. All lines represent 5-day averages. (For interpretation of the references to color in this figure legend, the reader is referred to the web version of this article.)

crops were not long enough to access that water. As a result of the warmer temperatures and lower soil water content in 2015, high VPD values (~ 1800 Pa) were reached at both sites during the growing season. In contrast, the growing season in 2016 was characterized by lower PPF, lower air temperature and lower VPD, while soil water content was not depleted (Fig. 1).

3.2. Annual cycles in GPP and SIF under different environmental conditions

GPP and SIF had similar overall annual cycles in 2015 and 2016 at the Lägeren site, although with some marked differences (Fig. 2). The peak in GPP and SIF for the growing seasons at Lägeren corresponded well in 2015 and 2016, with an earlier and smaller peak of $10 \text{ g C m}^{-2} \text{ d}^{-1}$ for GPP and $0.5 \text{ mW m}^{-2} \text{ sr}^{-1} \text{ nm}^{-1}$ for SIF in late May/early June 2015, while in 2016 the peak was later in June, with $12 \text{ g C m}^{-2} \text{ d}^{-1}$ for GPP and $1.1 \text{ mW m}^{-2} \text{ sr}^{-1} \text{ nm}^{-1}$ for SIF. The dry and warm climate in 2015 ($+2^\circ\text{C}$, -47% rain; Fig. 1) led to a strong decrease in productivity, starting in late June 2015, and this continued for most of the summer, while such reductions were not seen in 2016 due to the more favorable weather conditions. However, annual cycles of GPP and SIF also markedly diverged at the Lägeren site, with a narrower range of months for SIF emissions and with almost no SIF emission outside the main growing season from September to April. This divergence in the GPP and SIF annual cycles was due to differences in the footprint sizes from the EC system and the spectrometer. Indeed, the footprint of the UniSpec-DC spectrometer at the Lägeren site is about 3 trees ($\sim 10 \text{ m}^2$), while GPP derived from the EC system integrates over approximately 200 m^2 during daytime. This difference in footprints is especially important in a mixed forest like Lägeren, because the signal depends on which species the spectrometer measures. As a result, the tower-based UniSpec-DC spectrometer successfully measured SIF, however, mostly from about 3 beech trees below the spectrometer. During the year 2015, these beech trees were affected by the heat wave as well as by an aphid infestation, which made the induced-leaves senesce already in July. This can be seen by the abrupt decrease in SIF starting in June 2015 ($\sim 50\%$) with no more SIF emissions by mid-July (Fig. 2b).

The annual courses of GPP and SIF differed at the Oensingen

cropland site due to different climate and crop types (Fig. 3). In 2015, the main crop during the growing season was winter barley, with peaks in GPP of $14 \text{ g C m}^{-2} \text{ d}^{-1}$ and in SIF of $3.5 \text{ mW m}^{-2} \text{ sr}^{-1} \text{ nm}^{-1}$ in early May. During the 2015 winter, the winter barley crop was already established and was green, leading to a SIF signal from steady-state emissions (Lichtenthaler and Rinderle, 1988). The barley crop ripened and senesced in June until the harvest in early July. There was also a second peak in the GPP signal in September, representing the cover crop. However, the cover crop in the footprint of the UniSpec-DC spectrometer did not establish well, so this peak was not reflected in the SIF signal. In 2016, the main crop was pea, which did not grow well due to a very wet spring (Fig. 1) that affected a lot of croplands in Switzerland. The pea crop at Oensingen never fully recovered from this wet spring and had a very low productivity during the whole growing season, with peaks in productivity of only $7 \text{ g C m}^{-2} \text{ d}^{-1}$ for GPP and of $0.8 \text{ mW m}^{-2} \text{ sr}^{-1} \text{ nm}^{-1}$ for SIF in July. Overall, GPP and SIF had more similar shaped annual cycles at the Oensingen site than at the Lägeren mixed forest, indicating the advantage of a uniform footprint area. However, the correspondence of footprint sizes remains also crucial for homogenous canopies.

3.3. Diurnal cycles in GPP and SIF under different environmental conditions

Diurnal cycles were examined at the Lägeren forest site and at the Oensingen cropland site to understand differences in GPP and SIF on an hourly time scale. In March and April 2016 at the Lägeren forest site, GPP reached values of about $10 \mu\text{mol m}^{-2} \text{ s}^{-1}$, while SIF was still near $0 \text{ mW m}^{-2} \text{ sr}^{-1} \text{ nm}^{-1}$ (Fig. 4a and b). During these two months, the uptake from GPP came from the understorey vegetation and the spruce trees, as the deciduous trees had not yet leafed out. The tower-based spectrometer could therefore not measure any of these plants, as they were not in the footprint. During May to August, GPP reached diurnal peaks of 20 to $30 \mu\text{mol m}^{-2} \text{ s}^{-1}$, mostly following the incoming PPF (Fig. 4c to f). SIF followed similar diurnal cycles, with peaks of 0.6 to $0.8 \text{ mW m}^{-2} \text{ sr}^{-1} \text{ nm}^{-1}$ (Fig. 4c to f). A lag in SIF emissions was found in early morning and late afternoon compared to GPP due to structural effects (e.g. low sun illumination angles and hence very little volumetric scattering within the canopy) and topographical effects (Lägeren

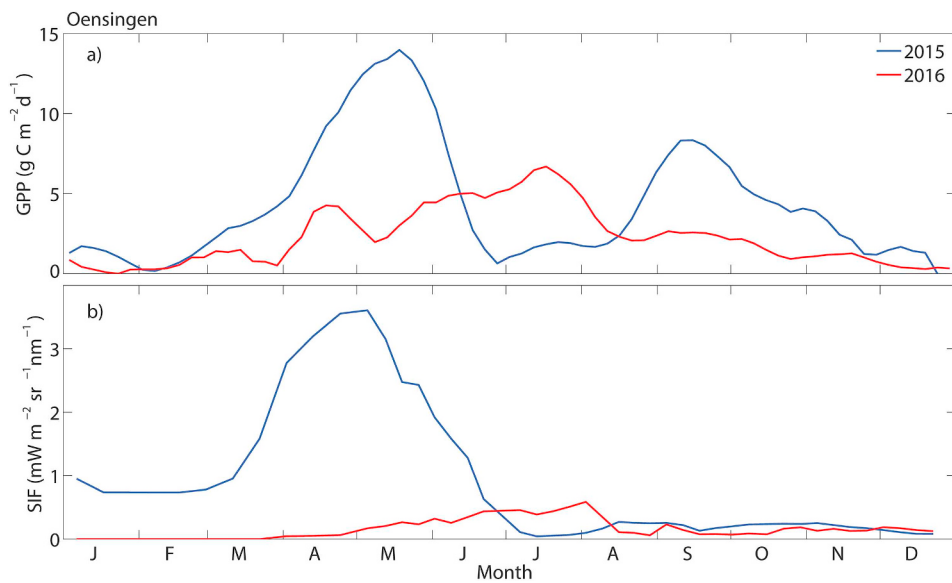


Fig. 3. Gross primary production (GPP, panel a) and sun-induced fluorescence (SIF, panel b) at the Oensingen cropland site in 2015 (winter barley, cover crop; blue line) and 2016 (peas; red line). All lines represent 5-day averages. (For interpretation of the references to color in this figure legend, the reader is referred to the web version of this article.)

is located on a south facing slope, resulting in shading in early morning and late afternoon). In addition, during May to August, a reduction in SIF of 50 to 80% was measured at midday to mid-afternoon, often between 13:00 and 16:00 h (Fig. 4c to f). This reduction was also partly seen in the GPP signal in the months from June to August, although to a much lower extent (reduction of 10 to 30%) (Fig. 4d to f). This reduction in SIF was synchronized with peak VPD values following peak PPFD (Fig. 4c to f).

At the Oensingen cropland site in 2015, the growth of the winter barley started in March and highest growth rates occurred in April and May (Fig. 5a to c). GPP and SIF followed similar diurnal cycles in March and April 2015 (Fig. 5a and b). GPP peaked around 12 and 20 $\mu\text{mol m}^{-2} \text{s}^{-1}$, while SIF peaked around 0.4 and

1 $\text{mW m}^{-2} \text{sr}^{-1} \text{nm}^{-1}$ (Fig. 5a and b). GPP and SIF followed the incoming PPFD. Strong reductions in SIF (60 to 90%) were measured in May and June around midday, often between 10:00 to 15:00 h (Fig. 5c and d), as seen previously at the Lägeren site under high VPD conditions. These SIF reductions occurred under peak PPFD (Fig. 5). Field observations during the 2015 growing season showed that the crops were downregulating photosynthesis during that time of the day, wilting for a few hours under this high insolation. It is also important to note that the barley crop in June 2015 had developed a layer of non-fluorescing ears, and we cannot rule out at this point that this complex vertical structure caused part of the SIF decrease around noon (Fig. 5d). In July 2015, the winter barley became senescent during ripening and thereby did not photosynthesize much until it was harvested. In August

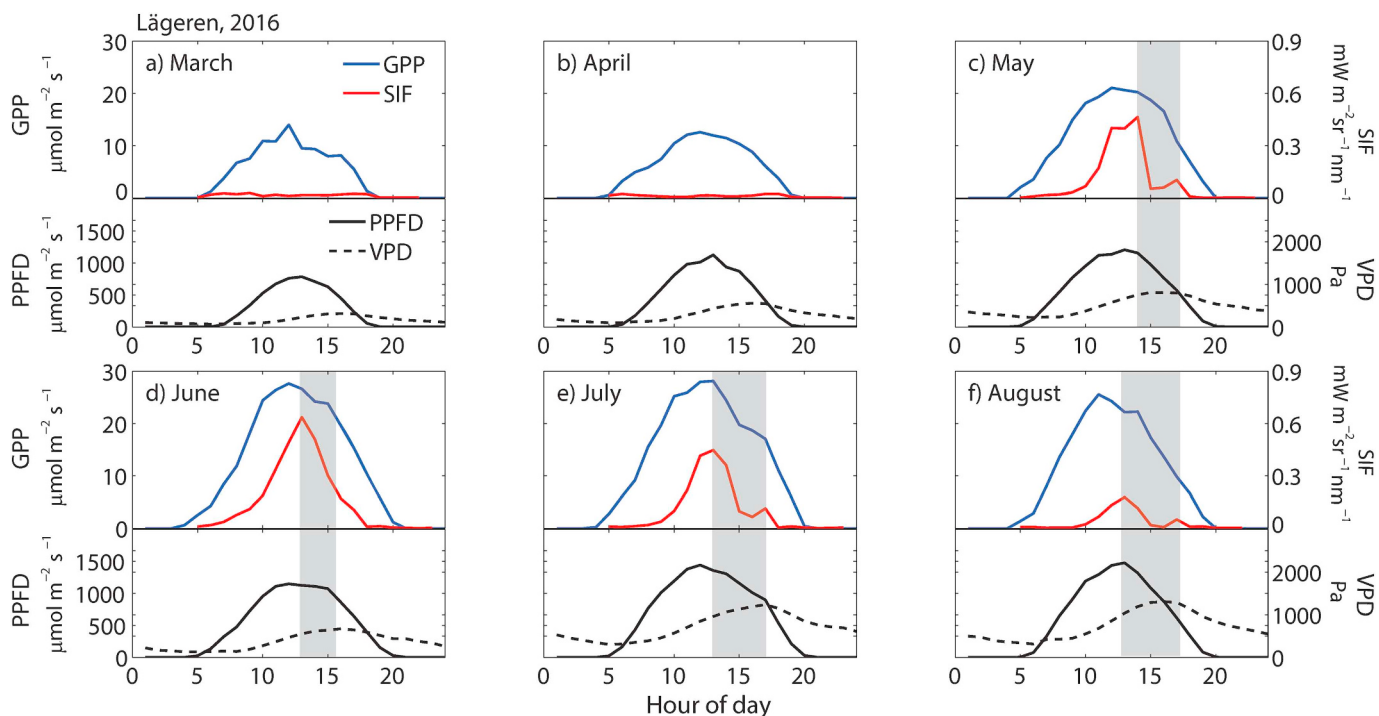


Fig. 4. Ensemble mean monthly diurnal GPP (blue line), SIF (red line), PPFD (black line) and VPD (dashed line) for a) March, b) April, c) May, d) June, e) July and f) August at the Lägeren mixed forest site in 2016. The shaded area represents the midday depression in SIF. (For interpretation of the references to color in this figure legend, the reader is referred to the web version of this article.)

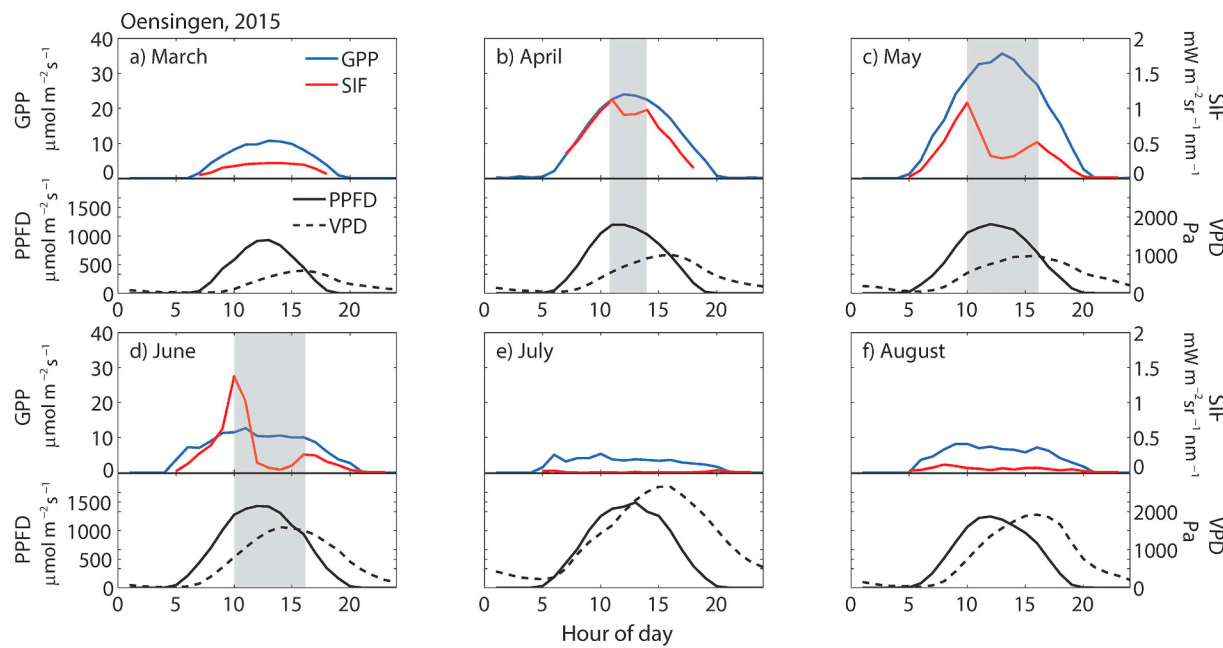


Fig. 5. Ensemble mean monthly diurnal GPP (blue line), SIF (red line), PPFD (black line) and VPD (dashed line) for a) March, b) April, c) May, d) June, e) July and f) August at the Oensingen cropland in 2015 (winter barley and cover crop). The shaded area represents the midday depression in SIF. (For interpretation of the references to color in this figure legend, the reader is referred to the web version of this article.)

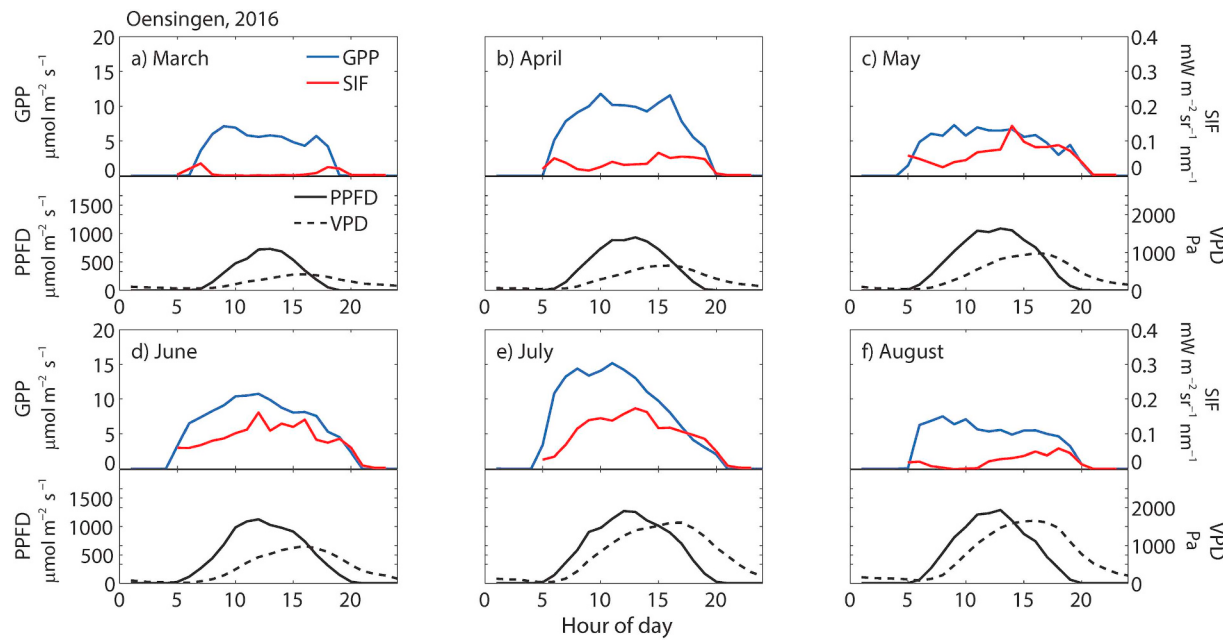


Fig. 6. Ensemble mean monthly diurnal GPP (blue line), SIF (red line), PPFD (black line) and VPD (dashed line) for a) March, b) April, c) May, d) June, e) July and f) August at the Oensingen cropland (pea crop) in 2016. (For interpretation of the references to color in this figure legend, the reader is referred to the web version of this article.)

2015, the field consisted of the barley stubble and a few emerging weeds.

In contrast, the pea crop in 2016 had low productivity over the full growing season (Fig. 3), mainly due to bad crop establishment caused by the cloudy and wet conditions, particularly in spring (Fig. 1). This was reflected in both GPP and SIF signals. GPP reached maximum values of $15 \mu\text{mol m}^{-2} \text{s}^{-1}$, only about half of GPP compared to those of winter barley, while SIF reached a maximum of $0.2 \text{ mW m}^{-2} \text{sr}^{-1} \text{nm}^{-1}$ (Fig. 6). The soil water content was high throughout the growing season ($> 30\%$), while PPFD and VPD were lower than in 2015 (Fig. 1). No midday depression was measured during the 2016 growing season

(Fig. 6). The crop was senescent in July and was harvested on July 25th. In August, the field was mostly empty except for some sparse remaining weeds following the harvest, which contributed to the GPP.

3.4. Environmental controls on SIF

Different environmental controls caused the SIF reductions at the Oensingen cropland site and at the Lägeren forest site. At the Oensingen cropland site in 2015, the SIF depression occurred around midday and was associated with high PPFD and high VPD (Fig. 7a and c). SIF increased with PPFD until a threshold of $1470 \mu\text{mol m}^{-2} \text{s}^{-1}$, where SIF

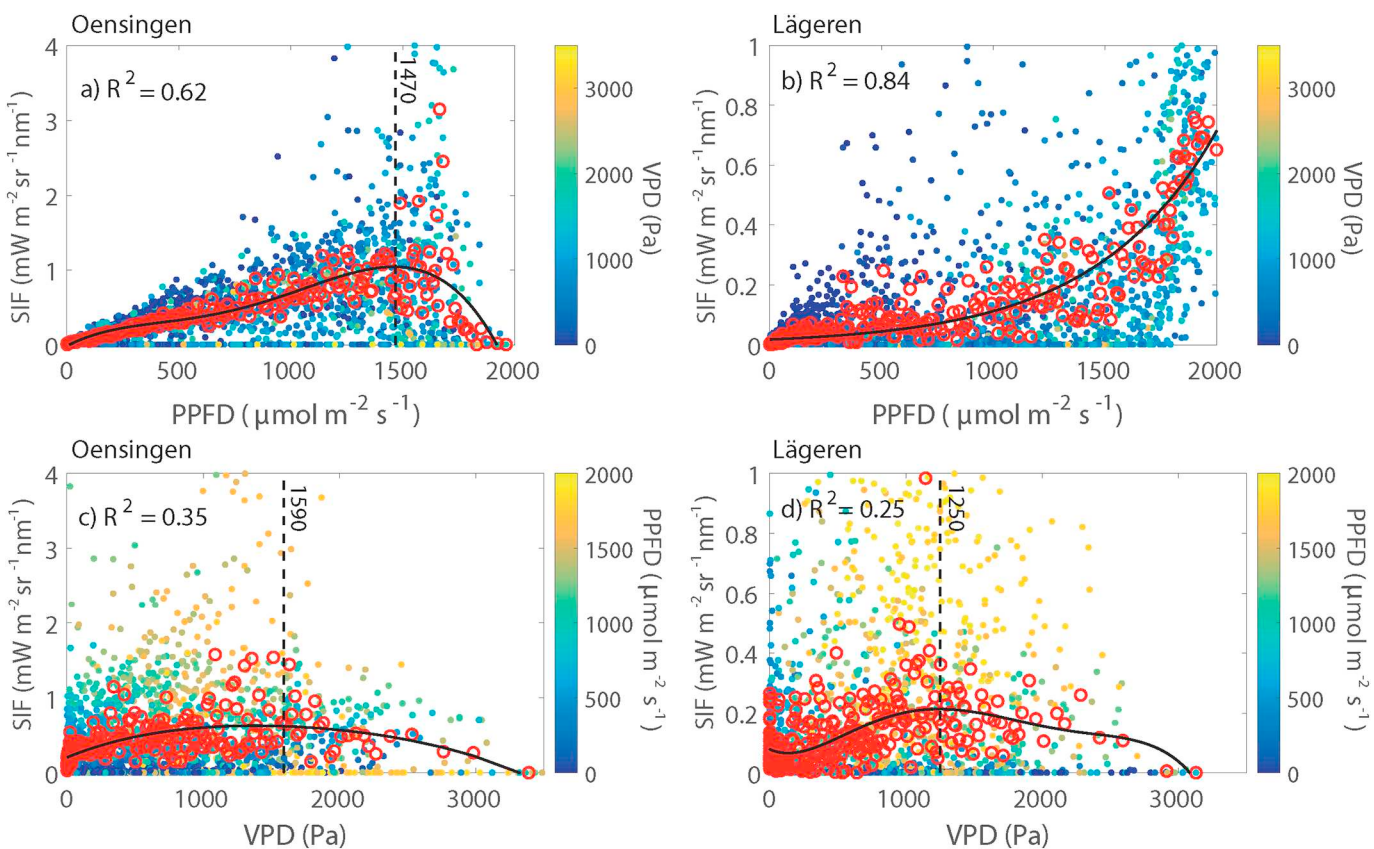


Fig. 7. Relationships during the growing season between SIF and PPFD for a) Oensingen and b) Lägeren, and relationships between SIF and VPD for c) Oensingen and d) Lägeren. The color of the dots in the top panels represent VPD, and in the bottom panels represent PPFD. The blue to yellow dots show the raw half-hourly data while the red circles show the data binned by increments of 10 values. The dashed line represents the threshold after which the relationship is negative for panel a) at 1470 $\mu\text{mol m}^{-2} \text{s}^{-1}$, for panel c) at 1590 Pa and for panel d) at 1250 Pa. The thresholds were determined using local maxima before negative trends in the curves. The equations for the fits can be found in Table 1. (For interpretation of the references to color in this figure legend, the reader is referred to the web version of this article.)

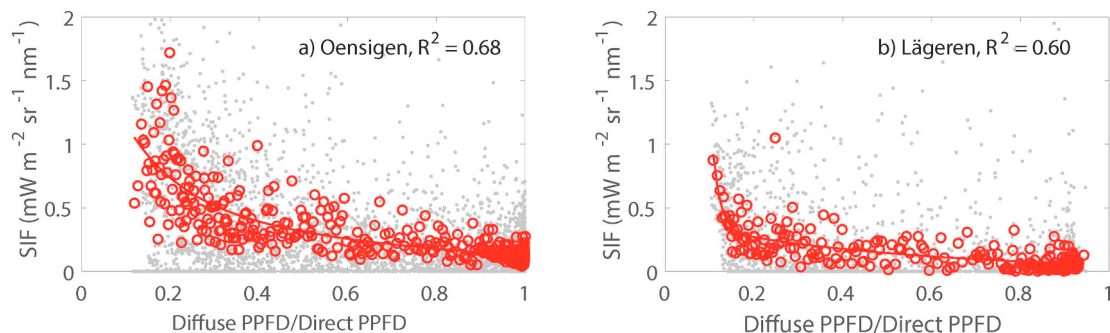


Fig. 8. SIF as a function of the ratio of diffuse to direct PPFD during the growing seasons in 2015 and 2016 at a) Oensingen and b) Lägeren. The equations for the fit can be found in Table 2.

started to decrease ($R^2 = 0.62$, Fig. 7a). In addition, SIF values decreased when VPD reached a threshold of 1590 Pa ($R^2 = 0.35$, Fig. 7c). At the Lägeren forest site, the SIF depression occurred later in the afternoon and was linked to high VPD values ($\text{VPD} > 1250 \text{ Pa}$, $R^2 = 0.25$, Fig. 7d). Higher PPFD values were however not linked to lower SIF values like at the cropland site, but rather to higher SIF values ($R^2 = 0.84$, Fig. 7b). Similar environmental controls were found for GPP at both sites (Fig. S 2). SIF values tended to slightly increase with a decreasing ratio of diffuse to direct PPFD, and this increase sharpened at a ratio below 0.3 (i.e., under clearer sky conditions with mostly direct light), where higher SIF values were found in addition to greater scatter at both sites (Fig. 8).

3.5. Relationship between SIF and NPQ

The relationship between energy emission by SIF and the photochemical reflectance index (PRI), an indicator for energy dissipation as heat through non-photochemical quenching (NPQ), was investigated to understand if times with SIF depressions showed high NPQ. On a diurnal basis, SIF and PRI were negatively correlated ($R^2 = 0.78$), with PRI values becoming increasingly negative as SIF values became increasingly positive (Fig. 9, top panels). Low SIF emissions during the midday/afternoon depression were associated with an increase in PRI, leading to peak values in PRI during that time (Fig. 9, top panels). It is particularly interesting that the start of the SIF emission decline was

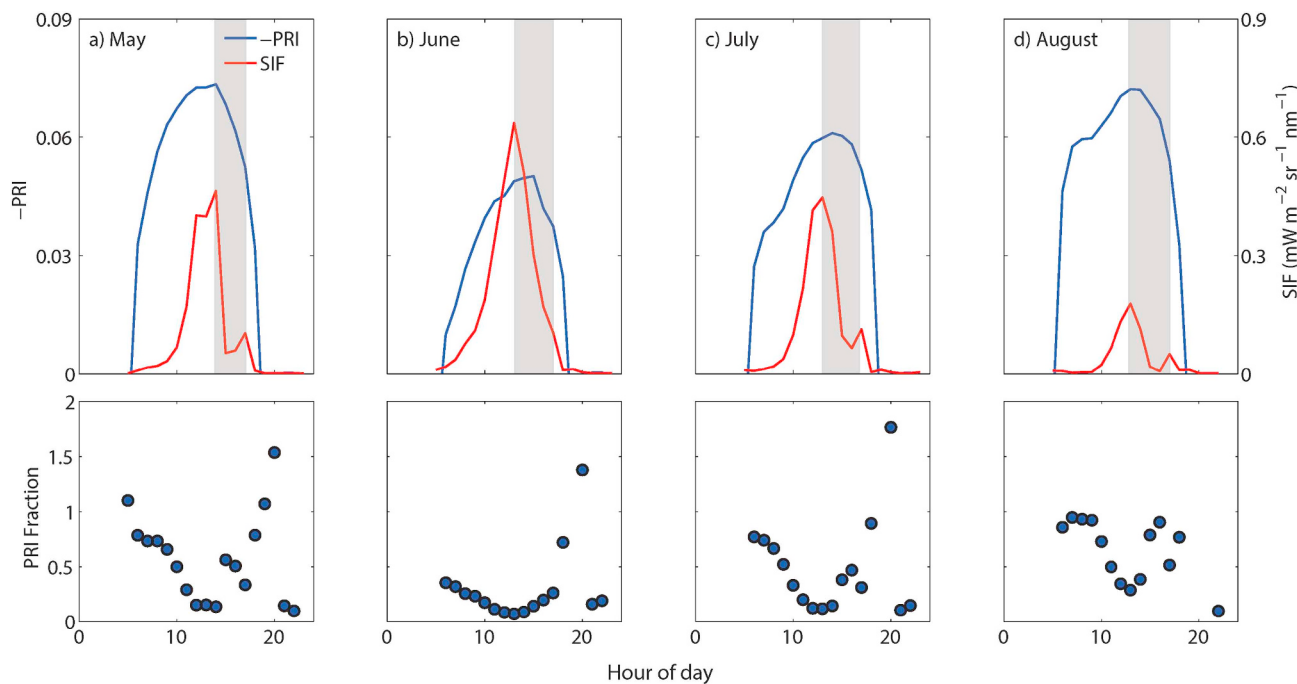


Fig. 9. Ensemble monthly diurnal cycles (top panels) in photochemical reflectance index (-PRI) (blue line) and SIF (red line) for a) May, b) June, c) July and d) August in 2016 at the Lägeren mixed forest site. Please note that -PRI is plotted in the top panel to facilitate the comparison with SIF. Fraction of energy allocated to non-photochemical quenching (NPQ) as indicated by PRI Fraction (bottom panels). The gray bands show depressions in SIF linked to peak in -PRI. (For interpretation of the references to color in this figure legend, the reader is referred to the web version of this article.)

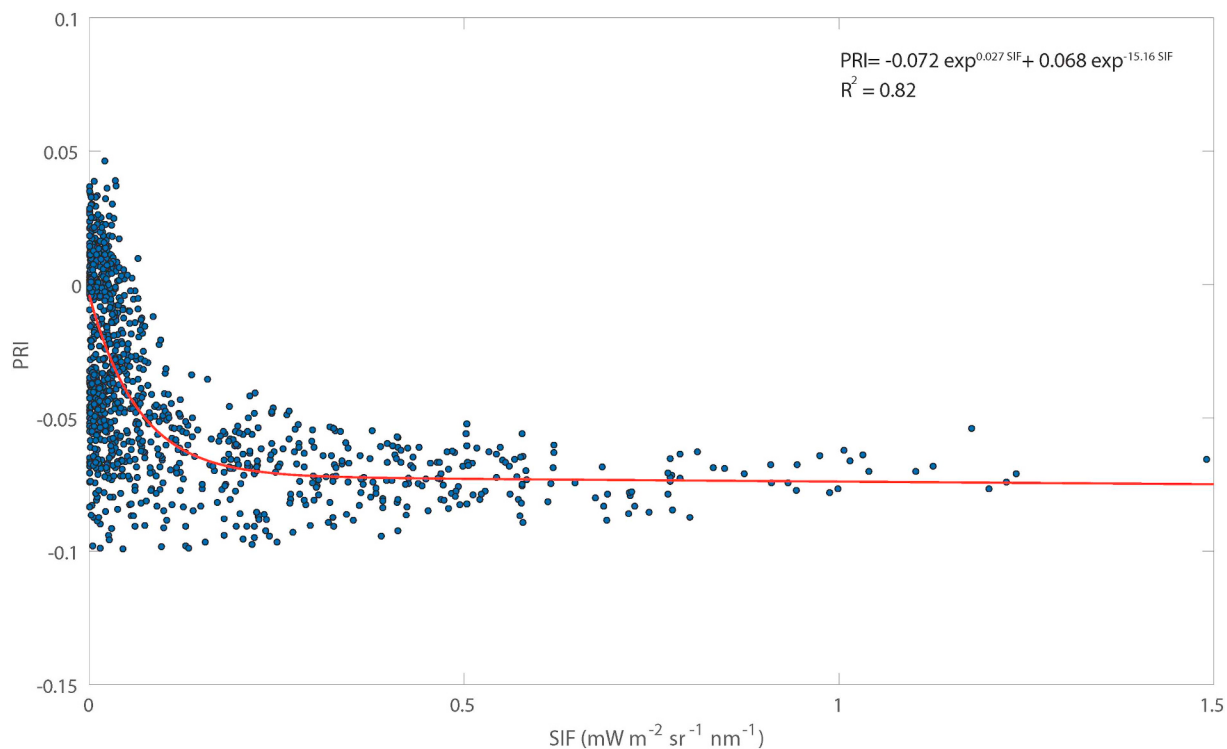


Fig. 10. Half-hourly PRI vs. SIF values at the Lägeren mixed forest in 2016. The blue circles represent half-hourly values and the red line is the fitted decaying exponential relationship. (For interpretation of the references to color in this figure legend, the reader is referred to the web version of this article.)

associated with peaking PRI values, while a small recovery of SIF emissions happened later with reduced PRI (Fig. 9, top panels). The fraction of NPQ to the total non-photosynthetic energy dissipation was found to increase during the midday/afternoon depression in SIF (Fig. 9, bottom panels). PRI was also found to represent a greater

fraction of the total energy dissipation in May and August than in June and July (Fig. 9). On a half-hourly basis, PRI values were found to be more positive when SIF values were low and more negative when SIF emissions were high (Fig. 10). These results therefore suggested a shift from SIF emissions under normal condition to some NPQ heat release

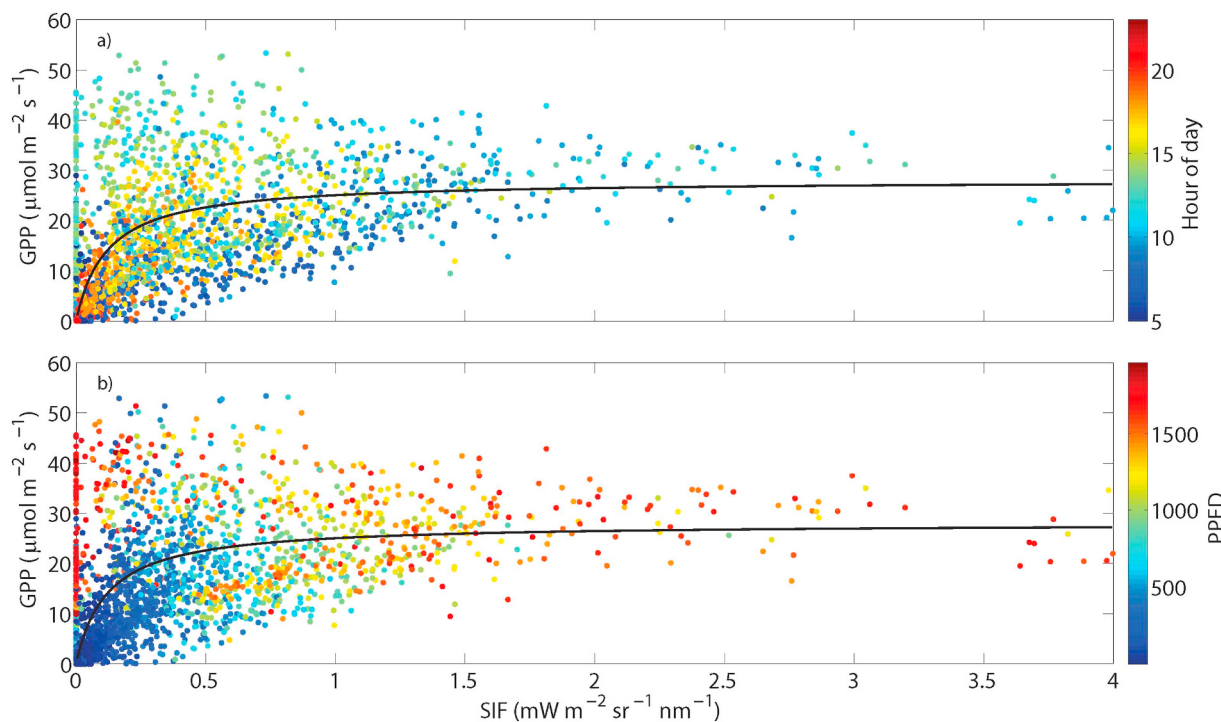


Fig. 11. Functional relationship between half-hourly GPP and SIF classified by a) hour of day and b) PPFD for the barley crop at the Oensingen cropland site in 2015. (For interpretation of the references to color in this figure, the reader is referred to the web version of this article.)

under stressful environmental conditions leading to the midday depression.

3.6. Functional relationships between GPP and SIF

As a result of the influence of environmental conditions on SIF, the functional relationships between GPP and SIF are likely to vary depending on the time of measurements and on the environmental conditions at that time. As can be seen in Fig. 11a for the barley crop at Oensingen, the variations in the relationship between GPP and SIF created considerable scatter on an annual basis, especially around midday (light blue points) when plants became light saturated ($\text{PPFD} > 1470 \mu\text{mol m}^{-2} \text{s}^{-1}$, Fig. 7a). This can also be seen in Fig. 11b where for high incoming PPFD (red points), different relationships were found depending on if the midday depression had occurred or not. Fig. 11b shows that before the midday depression, GPP and SIF were related in a hyperbolic way, while after the midday depression SIF values tend to reduce near $0 \text{ mW m}^{-2} \text{sr}^{-1} \text{nm}^{-1}$.

These differences in SIF emissions under stressed or unstressed conditions for a certain ecosystem influence the daily SIF budgets, as when midday reduction occur the daily SIF budget will be much lower than without any midday depression. The stressful environmental conditions at the Oensingen cropland site in 2015 led to very different functional relationships between SIF and GPP under stressed and unstressed conditions, i.e., depending on occurrence or absence of the midday depression (Fig. 12a). The functional relationship was hyperbolic under unstressed conditions, while under stressed conditions a linear relationship was found due to the reduced SIF values around midday (Fig. 12a). In 2016, the pea crop had lower productivity and the SIF-GPP relationship could be defined by only one hyperbolic equation (Fig. 12b). At the Lägeren forest site, the same equation could be applied to daily averaged GPP and SIF for both years (Fig. 12c and d), as the plant species do not change between the growing seasons like at Oensingen. Relationships for plants on days with stressful conditions could also be explained by the same equation, being linked to lower SIF values (Fig. 12c and d).

4. Discussion

4.1. Midday depression in SIF

Midday to afternoon depressions in SIF were found in both ecosystems during the growing season. The different environmental controls and timings of the SIF depression in both ecosystems suggest different vegetation acclimations. At the Lägeren site, the reduction in SIF was synchronized with peak VPD values ($> 1250 \text{ Pa}$) following peak PPFD (Figs. 4 and 7), suggesting a stomatal response linked to high VPD and limited water supply. For the barley crop at Oensingen in 2015, these SIF reductions occurred under peak PPFD ($> 1470 \mu\text{mol m}^{-2} \text{s}^{-1}$) and high VPD ($> 1590 \text{ Pa}$), showing the reduced ability of crops to mitigate stress imposed by high light under high evaporative demand. In comparison, the pea crop at Oensingen in 2016 showed no midday depression as soil water content was high throughout the growing season combined with lower PPFD and VPD (Fig. 6). In addition, the pea crop had in general a very low productivity due to a wet spring resulting in poor crop establishment, and peak SIF and GPP photosynthetic rates were only about a half of those measured in 2015 (Figs. 3, 5 and 6). In both ecosystems, the ratio of diffuse to direct PPFD only had a small effect on SIF, except for clear sky conditions where higher SIF values and more scatter were found due to the presence or absence of light saturation for the photosynthetic system of the plants (Fig. 8). These results therefore show that the SIF depression is highly dependent on the ecosystems and environmental conditions.

Many studies measuring chlorophyll fluorescence at leaf level found midday reductions in fluorescence emissions (e.g. Martínez-Ferri et al., 2000; Pons and Welschen, 2003; Raschke and Resemann, 1986; Špunda et al., 2005; Xu and Shen, 2005; Zhang and Gao, 2000). This common phenomenon has been attributed to both stomatal and non-stomatal (i.e., photoinhibition of PS II) limitations under high light, high VPD, and/or high temperatures (e.g. Pons and Welschen, 2003; Xu and Shen, 2005; Zhang and Gao, 2000). Martínez-Ferri et al. (2000) found that drought-tolerant species exhibited a pronounced reduction in photochemical efficiency around midday, characterized by a decrease in the

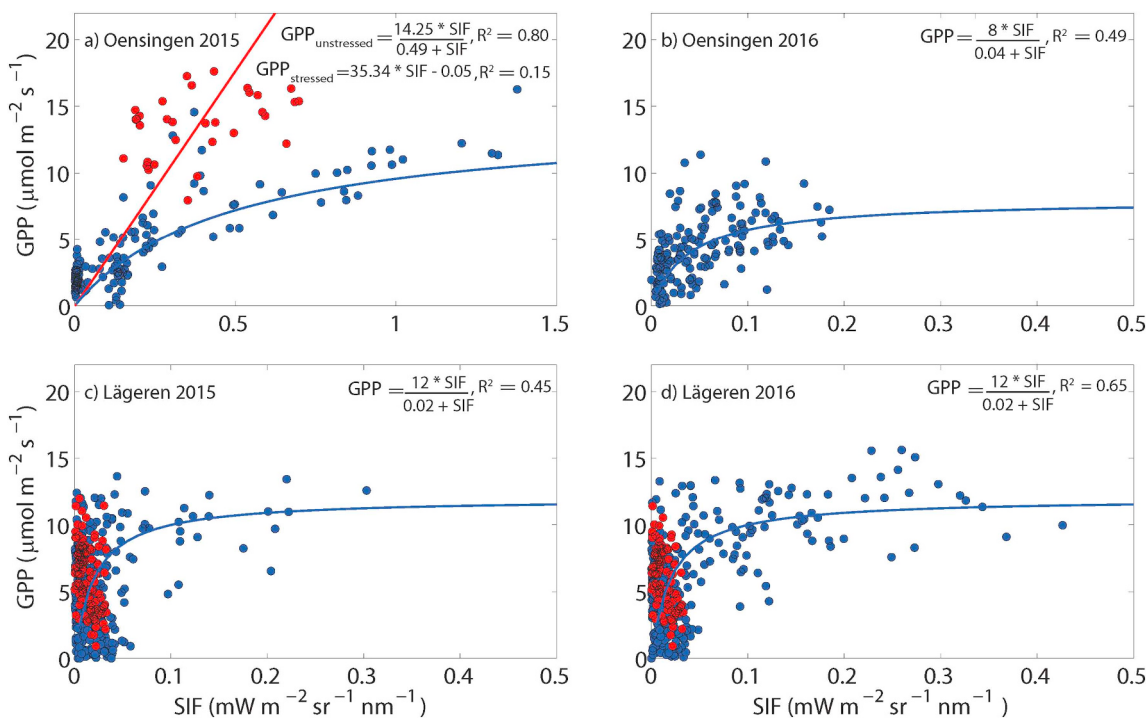


Fig. 12. Functional relationships between GPP and SIF at Oensingen cropland in a) 2015 for the barley crop and b) 2016 for the pea crop, and at the Lägeren mixed forest site in c) 2015 and d) 2016. The circles represent daily averages. Red circles characterize the stressful environmental conditions (i.e. days with PPFD > 1470 $\mu\text{mol m}^{-2} \text{s}^{-1}$ VPD > 1590 Pa at Oensingen and days with VPD > 1250 Pa at Lägeren). (For interpretation of the references to color in this figure legend, the reader is referred to the web version of this article.)

excitation capture efficiency of the open PS II centers, to avoid permanent photodamage. Midday depression in Norway spruce trees was linked to an increased contribution of non-stomatal processes due to the insufficiency of inorganic phosphate in the chloroplasts for adenosine diphosphate (ATP) synthesis and Ribulose-1,5-bisphosphate (RuBP) regeneration (Špunda et al., 2005). Others have found that the increased oxygenation of RuBP was not compensated by increases in carboxylation activity, likely due to the negative effect of high temperatures on Rubisco activity (Pons and Welschen, 2003). Raschke and Resemann (1986) found that depressions occurred if a threshold between 2000 and 3000 Pa in water-vapour pressure difference between the air and the leaf was exceeded. Thus, the depression measured in the SIF emission for both ecosystems in this study is therefore not a surprise from an ecophysiological point of view, although to our knowledge the midday depression in the SIF signal has not yet been reported or actively considered in remotely sensed SIF studies.

As SIF is emitted from the chlorophyll molecules of PS II, a decrease in productivity in PS II due to environmental pressure causes a chain of different protection mechanisms and eventually a decrease in SIF signal. Light, for example, is essential for photosynthesis, but too much light will result in accumulated non-utilised excitation energy, thus reducing the photosynthetic light efficiency (Demmig-Adams, 1990). Two pathways compete to de-excite the absorbed light energy that is not used in photochemistry: the energy can be either emitted as SIF or dissipated as heat through NPQ (Porcar-Castell et al., 2014). The fractions of absorbed light energy that flow along each of the two pathways are especially sensitive to stress conditions induced by environmental factors (Flexas and Medrano, 2002; Maxwell and Johnson, 2000). As a result, the functional link between SIF and GPP depends on the rate of NPQ and, consequently, is influenced by stress levels. The depression in SIF found in this study was associated with a peak in NPQ. Other studies have also found that decreases in SIF due to plant stress, especially under limited water supply, were linked to higher NPQ amounts (Li et al., 2000; Meroni et al., 2008; Peguero-Pina et al., 2008). In addition, the sharp increases/decreases in PRI in early morning and late

afternoon suggested a larger influence of vegetation structure and reflectance anisotropy on the PRI (Verrelst et al., 2008) than on SIF. Our results are also in agreement with model simulations presented in a recent study by Verrelst et al. (2015) who used the radiative transfer and energy balance model SCOPE (van der Tol et al., 2009a) and a photosynthesis module (MD12) providing an explicit parameterization of fluorescence quenching mechanisms by incorporating effects of PS II photoinhibition and sustained dark-adapted NPQ on photosynthesis and fluorescence. Results obtained from this model indicate a significant impact of NPQ and the fraction of functional reaction centers on SIF emissions. This combined effect can even become dominant if biochemical and structural canopy parameters do not change as for example over a day.

It is also important to mention at this point the influence of measurement techniques. In most cases, tower-based and airborne spectrometers will measure predominantly the top canopy leaves, which will be more sensitive to light saturation during midday/afternoon (Williams et al., 1996). Indeed, top canopy leaves are exposed to the highest atmospheric demands (i.e. high light, temperature and VPD) and hydraulic resistance (i.e. getting water from the roots once leaf and canopy supply are exhausted despite xylem hydraulic resistance) (Williams et al., 1996). In contrast, GPP partitioned from EC measurements integrate over the entire ecosystem and thus, are less likely to measure a depression as strong, as the leaves lower in the canopy will be less affected by light saturation and VPD limitations (Jones, 2014; Nobel et al., 1993). In this study, GPP was affected by the same ecosystem-specific environmental controls (i.e., VPD and PPFD for Oensingen, and VPD only for Lägeren) as SIF (Fig. S 2), although this was reflected less strongly in the diurnal cycles. A reduction of 10 to 30% could sometimes be seen in GPP, but never to the extent measured with SIF. Moreover, GPP derived from nighttime EC fluxes is known to be associated with large uncertainties when photoinhibition occur, as daytime leaf respiration is then reduced due to the inhibition (e.g. Brooks and Farquhar, 1985; Villar et al., 1995), resulting in an overestimation of both the partitioned GPP and respiration in such

conditions (e.g. Heskel et al., 2013; Janssens et al., 2001).

4.2. Tower-based SIF retrievals with medium spectral resolution

While the precise retrievals of SIF require data measured at sub-nanometer spectral ($< 0.3 \text{ nm}$) resolution (Guanter et al., 2013), many studies have demonstrated the reliability of spectrometers with a medium spectral resolution of about 3 nm for deriving SIF (Damm et al., 2010; Damm et al., 2011; Liu and Cheng, 2010; Meroni et al., 2009; Rascher et al., 2009), as the UniSpec-DC spectrometers used in this study. The estimated uncertainty in the values reported in this study due to the spectral resolution of the sensor is about 10% considering the 3FLD approach as applied in our study (Damm et al., 2011). Overall, the annual and diurnal cycles clearly demonstrated the ability of the UniSpec-DC to measure SIF, with the midday depression in SIF being an indication of the measurement of the activity in PS II. It must be noted that the measured reduction in SIF during midday can be caused by the observational setting as well: Geometric optical scattering can dominate the radiative transfer if sensors are too close to the canopy, causing shadowing effects that are only present in the upwelling radiance measurement but not the irradiance measurement. Since our instrumental setup was fixed and the midday depression in SIF occurs and diminishes (cf. Figs. 4–6) we can rule out such causes. In addition, Fig. S 3 shows that no shading effects could be seen in the irradiance and radiance components, thereby not being caused by reflectance/emittance anisotropy in first order.

A good agreement in GPP and SIF was found, demonstrating their close link, being both driven by the incoming PPF (Figs. 4, 5 and 6). The continuous tower-based UniSpec-DC measurements allowed us to get additional insights on how SIF reacts to plant stress. An advantage of tower-based SIF retrievals compared to those airborne or spaceborne is that they allow us to measure under all environmental conditions, with diffuse and direct light, and thus, give us a better indication of how the signals vary over time depending on environmental conditions, an information routinely available with partitioned GPP from EC flux towers. A limitation when comparing the tower-based SIF to EC-derived GPP was however the size of the footprint, which as we have seen in this study, had a larger influence in a mixed forest than in a uniform crop stand. On the other side, any validation approach of satellite-derived SIF and higher level products as for example envisaged for ESA's FLEX mission (Drusch et al., 2017) in homogeneous and heterogeneous canopies has to carefully consider aspects concerning footprints and physiological differences between the upper and whole canopy.

4.3. Implications for SIF measurements at regional to global scales

Despite studies showing that SIF from the Greenhouse Gases Observing Satellite (GOSAT) (Frankenberg et al., 2012) and Global Ozone Monitoring Mission-2 (GOME-2) (Joiner et al., 2014) were well correlated with GPP, the understanding of process-based relationships between SIF and GPP at such a coarse resolution ($> 40 \text{ by } 80 \text{ km}^2$) remains quite limited. Since 2014, OCO-2 has enabled SIF retrievals with a finer resolution of $1.3 \text{ by } 2.5 \text{ km}^2$ (Frankenberg et al., 2014). The finer resolution of OCO-2 has enabled the study of the effects of environmental conditions on the SIF retrievals (Verma et al., 2017). However, the temporal resolution with 14 measurements over two years in that study is still too low to characterize the effects of environmental conditions. Current SIF models assume diurnal cycles in SIF for healthy or unstressed plants without midday depression (van der Tol et al., 2016). High light and high VPD have been shown to be critical factors for the midday depression (e.g. Pathre et al., 1998; Pons and Welschen, 2003; Raschke and Resemann, 1986), although varying in extent depending on species-acclimation to drought stress (e.g. Martínez-Ferri et al., 2000; Pathre et al., 1998), and such reactions to stress would gain from being added to model-based SIF.

The midday depressions in SIF as measured in this study in a mixed

forest and a cropland might have consequences on SIF emissions measured globally for different ecosystems depending on the environmental conditions and on the time of the overpass of different satellites. It will be important to characterize how different ecosystems react to different environmental conditions to be able to account for these effects. Given that remote sensing measurements tend to represent snapshots in time, the consistency of the time of measurements can perhaps help to make comparisons, while keeping in mind that the entire picture is not reflected in these measurements. Furthermore, a sound interpretation of SIF and subsequent use to derive higher level products such as photosynthetic rates and CO_2 uptake rates require ingesting SIF observations along with information characterizing underlying vegetation and environmental conditions in process models (Lee et al., 2015; Parazoo et al., 2014; Parazoo et al., 2013). The FLEX mission concept thus makes an important step in this direction in providing an extensive set of information along with SIF to better describe photosynthesis and functioning of terrestrial vegetation (Drusch et al., 2017).

5. Conclusions

Environmental conditions were found to have an important effect on the SIF signal, especially under high light and high VPD conditions for the cropland site and under high VPD conditions for the forest site. Midday depression in fluorescence has been well studied in classical ecophysiological studies for more than 20 years, being a way for plants to avoid excess water loss and permanent photodamage, although to our knowledge no such depression has been yet measured in SIF-based remote sensing studies. The question remains as to whether this is missed when using snapshots in time or whether the effect becomes less relevant at a global scale. More studies looking into temporal dynamics of SIF-GPP relationships are needed to better understand the effect of environmental conditions and to reliably estimate GPP from remote sensing measurements.

Acknowledgements

This work was supported by a grant of the Swiss University Conference and the ETH Board within the KIP-5 project Swiss Earth Observatory Network (SEON). E. Paul-Limoges was also supported by a Natural Sciences and Engineering Research Council of Canada post-graduate scholarship. The contribution of M.E. Schaeppman is supported by the University of Zurich Research Priority Program on Global Change and Biodiversity. W. Eugster acknowledges support from the Swiss National Science Foundation (SNF) by grant 200021-146373. We are grateful to Thomas Baur, Florian Käslin, Philip Meier, Patrick Koller, Petra D'Odorico, Carmen Emmel and Lukas Hörtnagl for assistance in the field and in the laboratory. We thank Reto Maier for building the climate controlled enclosures for the spectrometers. Many thanks to Javier Pacheco-Labrador, Thomas Hilker and Zoran Nesic for sharing Matlab codes to control the UniSpec-DC and for providing helpful insights.

Appendix A. Supplementary data

Supplementary data to this article can be found online at <https://doi.org/10.1016/j.rse.2018.10.018>.

References

- Ač, A., Malenovský, Z., Olejníčková, J., Gallé, A., Rascher, U., Mohammed, G., 2015. Meta-analysis assessing potential of steady-state chlorophyll fluorescence for remote sensing detection of plant water, temperature and nitrogen stress. *Remote Sens. Environ.* 168, 420–436.
- Baldocchi, D.D., 2003. Assessing the eddy covariance technique for evaluating carbon dioxide exchange rates of ecosystems: past, present and future. *Glob. Chang. Biol.* 9, 479–492.
- Baldocchi, D., Falge, E., Gu, L.H., Olson, R., Hollinger, D., Running, S., Anthoni, P.,

- Bernhofer, C., Davis, K., Evans, R., Fuentes, J., Goldstein, A., Katul, G., Law, B., Lee, X.H., Malhi, Y., Meyers, T., Munger, W., Oechel, W., P.U.K.T., Pilegaard, K., Schmid, H.P., Valentini, R., Verma, S., Vesala, T., Wilson, K., Wofsy, S., 2001. FLUXNET: a new tool to study the temporal and spatial variability of ecosystem-scale carbon dioxide, water vapor, and energy flux densities. *Bull. Am. Meteorol. Soc.* 82, 2415–2434.
- Ballantyne, A., Smith, W., Anderegg, W., Kauppi, P., Sarmiento, J., Tans, P., Sheviakova, E., Pan, Y., Poulter, B., Anav, A., Friedlingstein, P., Houghton, R., Running, S., 2017. Accelerating net terrestrial carbon uptake during the warming hiatus due to reduced respiration. *Nat. Clim. Chang.* 7, 148–152.
- Barr, A.G., Black, T.A., Hogg, E.H., Kljun, N., Morgenstern, K., Nesic, Z., 2004. Inter-annual variability in the leaf area index of a boreal aspen-hazelnut forest in relation to net ecosystem production. *Agric. For. Meteorol.* 126, 237–255.
- Bear, C., Reichstein, M., Tomelleri, E., Ciais, P., Jung, M., Carvalhais, N., Rodenbeck, C., Arain, M.A., Baldocchi, D., Bonan, G.B., Bondeau, A., Cescatti, A., Lasslop, G., Lindroth, A., Lomas, M., Luysaert, S., Margolis, H., Oleson, K.W., Rouspud, O., Veenendaal, E., Viovy, N., Williams, C., Woodward, F.I., Papale, D., 2010. Terrestrial gross carbon dioxide uptake: global distribution and covariation with climate. *Science* 329, 834–838.
- Brooks, A., Farquhar, G., 1985. Effect of temperature on the CO₂/O₂ specificity of ribulose-1,5-bisphosphate carboxylase/oxygenase and the rate of respiration in the light. *Planta* 165, 397–406.
- Culver, M.E., Perry, M.J., 1997. Calculation of solar-induced fluorescence in surface and subsurface waters. *J. Geophys. Res. Oceans* 102, 10563–10572.
- Damm, A., Elbers, J.A.N., Erler, A., Gioli, B., Hamdi, K., Huitjes, R., Kosvancova, M., Meroni, M., Miglietta, F., Moersch, A., Moreno, J., Schickling, A., Sonnenschein, R., Udelhoven, T., Van Der Linden, S., Hostert, P., Rascher, U.W.E., 2010. Remote sensing of sun-induced fluorescence to improve modeling of diurnal courses of gross primary production (GP_P). *Glob. Chang. Biol.* 16, 171–186.
- Damm, A., Erler, A., Hillen, W., Meroni, M., Schaeppman, M.E., Verhoeft, W., Rascher, U., 2011. Modeling the impact of spectral sensor configurations on the FLD retrieval accuracy of sun-induced chlorophyll fluorescence. *Remote Sens. Environ.* 115, 1882–1892.
- Damm, A., Guanter, L., Laurent, V.C.E., Schaeppman, M.E., Schickling, A., Rascher, U., 2014. FLD-based retrieval of sun-induced chlorophyll fluorescence from medium spectral resolution airborne spectroscopy data. *Remote Sens. Environ.* 147, 256–266.
- Damm, A., Guanter, L., Paul-Limoges, E., van der Tol, C., Hueni, A., Buchmann, N., Eugster, W., Ammann, C., Schaeppman, M.E., 2015a. Far-red sun-induced chlorophyll fluorescence shows ecosystem-specific relationships to gross primary production: an assessment based on observational and modeling approaches. *Remote Sens. Environ.* 166, 91–105.
- Damm, A., Guanter, L., Verhoeft, W., Schlapfer, D., Garbari, S., Schaeppman, M.E., 2015b. Impact of varying irradiance on vegetation indices and chlorophyll fluorescence derived from spectroscopy data. *Remote Sens. Environ.* 156, 202–215.
- Demmig-Adams, B., 1990. Carotenoids and photoprotection in plants - a role for the xanthophyll zeaxanthin. *Biochim. Biophys. Acta* 1020, 1–24.
- Dietiker, D., Buchmann, N., Eugster, W., 2010. Testing the ability of the DNDC model to predict CO₂ and water vapour fluxes of a Swiss cropland site. *Agric. Ecosyst. Environ.* 139, 396–401.
- Dobrowski, S.Z., Pushnik, J.C., Zarco-Tejada, P.J., Ustin, S.L., 2005. Simple reflectance indices track heat and water stress-induced changes in steady-state chlorophyll fluorescence at the canopy scale. *Remote Sens. Environ.* 97, 403–414.
- Drolet, G.G., Middleton, E.M., Huemmrich, K.F., Hall, F.G., Amiro, B.D., Barr, A.G., Black, T.A., McCaughey, J.H., Margolis, H.A., 2008. Regional mapping of gross light-use efficiency using MODIS spectral indices. *Remote Sens. Environ.* 112, 3064–3078.
- Drusch, M., Moreno, J., Del Bello, U., Franco, R., Goulas, Y., Huth, A., Kraft, S., Middleton, E.M., Miglietta, F., Mohammed, G., Nedbal, L., Rascher, U., Schtttemeyer, D., Verhoeft, W., 2017. The Fluorescence EXplorer mission concept-ESA's Earth explorer 8. *IEEE Trans. Geosci. Remote Sens.* 55, 1273–1284.
- Etzold, S., Ruehr, N.K., Zweifel, R., Dobbertin, M., Zingg, A., Pluess, P., Hasler, R., Eugster, W., Buchmann, N., 2011. The carbon balance of two contrasting mountain forest ecosystems in Switzerland: similar annual trends, but seasonal differences. *Ecosystems* 14, 1289–1309.
- Eugster, W., Zeyer, K., Zeeman, M., Michna, P., Zingg, A., Buchmann, N., Emmenegger, L., 2007. Methodical study of nitrous oxide eddy covariance measurements using quantum cascade laser spectrometry over a Swiss forest. *Biogeosciences* 4, 927–939.
- Evain, S., Flexas, J., Moya, I., 2004. A new instrument for passive remote sensing: 2. Measurement of leaf and canopy reflectance changes at 531 nm and their relationship with photosynthesis and chlorophyll fluorescence. *Remote Sens. Environ.* 91, 175–185.
- Flexas, J., Medrano, H., 2002. Drought-inhibition of photosynthesis in C₃ plants: stomatal and non-stomatal limitations revisited. *Ann. Bot.* 89, 183–189.
- Flexas, J., Briantais, J.M., Cerovic, Z., Medrano, H., Moya, I., 2000. Steady-state and maximum chlorophyll fluorescence responses to water stress in grapevine leaves: a new remote sensing system. *Remote Sens. Environ.* 73, 283–297.
- Flexas, J., Escalona, J.M., Evain, S., Gualas, J., Moya, I., Osmond, C.B., Medrano, H., 2002. Steady-state chlorophyll fluorescence (Fs) measurements as a tool to follow variations of net CO₂ assimilation and stomatal conductance during water-stress in C₃ plants. *Physiol. Plant.* 114, 231–240.
- Foken, T., Göckede, M., Mauder, M., Mahrt, L., Amiro, B., Munger, W., 2005. Post-field data quality control. In: Lee, X., Massman, W., Law, B. (Eds.), *Handbook of Micrometeorology*. Springer, Netherlands, pp. 181–208.
- Frankenberg, C., O'Dell, C., Guanter, L., McDuffie, J., 2012. Remote sensing of near-infrared chlorophyll fluorescence from space in scattering atmospheres: implications for its retrieval and interferences with atmospheric CO₂ retrievals. *Atmos. Meas. Tech.* 5, 2081–2094.
- Frankenberg, C., O'Dell, C., Berry, J., Guanter, L., Joiner, J., Kohler, P., Pollock, R., Taylor, T.E., 2014. Prospects for chlorophyll fluorescence remote sensing from the Orbiting Carbon Observatory-2. *Remote Sens. Environ.* 147, 1–12.
- Friedlingstein, P., Cox, P., Betts, R., Bopp, L., Von Bloh, W., Brovkin, V., Cadule, P., Doney, S., Eby, M., Fung, I., 2006. Climate–carbon cycle feedback analysis: results from the C4MIP model intercomparison. *J. Clim.* 19, 3337–3353.
- Gamon, J.A., Penuelas, J., Field, C.B., 1992. A narrow-waveband spectral index that tracks diurnal changes in photosynthetic efficiency. *Remote Sens. Environ.* 41, 35–44.
- Gamon, J.A., Huemmrich, K.F., Wong, C.Y.S., Ensminger, I., Garrity, S., Hollinger, D.Y., Noormets, A., Penuelas, J., 2016. A remotely sensed pigment index reveals photosynthetic phenology in evergreen conifers. *Proc. Natl. Acad. Sci. U. S. A.* 113, 13087–13092.
- Garbulsky, M.F., Filella, I., Verger, A., Penuelas, J., 2014. Photosynthetic light use efficiency from satellite sensors: from global to Mediterranean vegetation. *Environ. Exp. Bot.* 103, 3–11.
- Guanter, L., Rossini, M., Colombo, R., Meroni, M., Frankenberg, C., Lee, J.-E., Joiner, J., 2013. Using field spectroscopy to assess the potential of statistical approaches for the retrieval of sun-induced chlorophyll fluorescence from ground and space. *Remote Sens. Environ.* 133, 52–61.
- Guanter, L., Zhang, Y., Jung, M., Joiner, J., Voigt, M., Berry, J.A., Frankenberg, C., Huete, A.R., Zarco-Tejada, P., Lee, J.E., Moran, M.S., Ponce-Campos, G., Beer, C., Camps-Valls, G., Buchmann, N., Gianelle, D., Klumpp, K., Cescatti, A., Baker, J.M., Griffis, T.J., 2014. Global and time-resolved monitoring of crop photosynthesis with chlorophyll fluorescence. *Proc. Natl. Acad. Sci. U. S. A.* 111, E1327–E1333.
- Heskell, M.A., Atkin, O.K., Turnbull, M.H., Griffin, K.L., 2013. Bringing the Kok effect to light: a review on the integration of daytime respiration and net ecosystem exchange. *Ecosphere* 4, 1–14.
- Janssens, I., Lankreijer, H., Matteucci, G., Kowalski, A., Buchmann, N., Epron, D., Pilegaard, K., Kutsch, W., Longdoz, B., Grünwald, T., 2001. Productivity overshadows temperature in determining soil and ecosystem respiration across European forests. *Glob. Chang. Biol.* 7, 269–278.
- Joiner, J., Yoshida, Y., Vasilkov, A., Schaefer, K., Jung, M., Guanter, L., Zhang, Y., Garrity, S., Middleton, E.M., Huemmrich, K.F., Gu, L., Marchesini, L.B., 2014. The seasonal cycle of satellite chlorophyll fluorescence observations and its relationship to vegetation phenology and ecosystem atmosphere carbon exchange. *Remote Sens. Environ.* 152, 375–391.
- Jones, H.G., 2014. *Plants and Microclimate: A Quantitative Approach to Environmental Plant Physiology*, 3rd ed. Cambridge University Press.
- Knorr, W., 2009. Is the airborne fraction of anthropogenic CO₂ emissions increasing? *Geophys. Res. Lett.* 36.
- Le Quéré, C., Andres, R.J., Boden, T., Conway, T., Houghton, R.A., House, J.I., Marland, G., Peters, G.P., Van der Werf, G., Ahlström, A., 2012. The global carbon budget 1959–2011. *Earth Syst. Sci. Data Discuss.* 5, 1107–1157.
- Le Quéré, C., Moriarty, R., Andrew, R.M., Peters, G.P., Ciais, P., Friedlingstein, P., Jones, S.D., Sitch, S., Tans, P., Arneth, A., 2015. Global carbon budget 2014. *Earth Syst. Sci. Data* 7, 47–85.
- Lee, J.-E., Frankenberg, C., van der Tol, C., Berry, J.A., Guanter, L., Boyce, C.K., Fisher, J.B., Morrow, E., Worden, J.R., Asefi, S., 2013. Forest productivity and water stress in Amazonia: observations from GOSAT chlorophyll fluorescence. *Proc. R. Soc. Lond. B Biol. Sci.* 280, 20130171.
- Lee, J.E., Berry, J.A., Van der Tol, C.S., Yang, X., Guanter, L., Damm, A., Baker, I., Frankenberg, C., 2015. Simulations of chlorophyll fluorescence incorporated into the community land model version 4. *Glob. Chang. Biol.* 21, 3469–3477.
- Li, X.P., Björkman, O., Shih, C., Grossman, A.R., Rosenquist, M., Jansson, S., Niyogi, K.K., 2000. A pigment-binding protein essential for regulation of photosynthetic light harvesting. *Nature* 403, 391–395.
- Li, X., Xiao, J.F., He, B.B., 2018. Chlorophyll fluorescence observed by OCO-2 is strongly related to gross primary productivity estimated from flux towers in temperate forests. *Remote Sens. Environ.* 204, 659–671.
- Lichtenthaler, H.K., Rinderle, U., 1988. The role of chlorophyll fluorescence in the detection of stress conditions in plants. *CRC Crit. Rev. Anal. Chem.* 19, S29–S85.
- Liu, L., Cheng, Z., 2010. Detection of vegetation light-use efficiency based on solar-induced chlorophyll fluorescence separated from canopy radiance spectrum. *IEEE J. Sel. Top. Appl. Earth Obs. Remote Sens.* 3, 306–312.
- Maier, S.W., Günther, K.P., Stellmes, M., 2003. Sun-induced fluorescence: a new tool for precision farming. In: *Digital Imaging and Spectral Techniques: Applications to Precision Agriculture and Crop Physiology*, pp. 209–222.
- Martínez-Ferri, E., Balaguer, L., Valladares, F., Chico, J., Manrique, E., 2000. Energy dissipation in drought-avoiding and drought-tolerant tree species at midday during the Mediterranean summer. *Tree Physiol.* 20, 131–138.
- Maxwell, K., Johnson, G.N., 2000. Chlorophyll fluorescence—a practical guide. *J. Exp. Bot.* 51, 659–668.
- Mercado, L.M., Bellouin, N., Sitch, S., Boucher, O., Huntingford, C., Wild, M., Cox, P.M., 2009. Impact of changes in diffuse radiation on the global land carbon sink. *Nature* 458, 1014–U1087.
- Meroni, M., Picchi, V., Rossini, M., Cogliati, S., Panigada, C., Nali, C., Lorenzini, G., Colombo, R., 2008. Leaf level early assessment of ozone injuries by passive fluorescence and photochemical reflectance index. *Int. J. Remote Sens.* 29, 5409–5422.
- Meroni, M., Rossini, M., Guanter, L., Alonso, L., Rascher, U., Colombo, R., Moreno, J., 2009. Remote sensing of solar-induced chlorophyll fluorescence: review of methods and applications. *Remote Sens. Environ.* 113, 2037–2051.
- Morales, F., Abadia, A., Abadia, J., 1990. Characterization of the xanthophyll cycle and other photosynthetic pigment changes induced by iron-deficiency in sugar-beet (*Beta-vulgaris* L.). *Plant Physiol.* 94, 607–613.
- Moya, I., Camenen, L., Evain, S., Goulas, Y., Cerovic, Z.G., Latouche, G., Flexas, J., Onnis,

- A., 2004. A new instrument for passive remote sensing 1. Measurements of sunlight-induced chlorophyll fluorescence. *Remote Sens. Environ.* 91, 186–197.
- Nemani, R.R., Keeling, C.D., Hashimoto, H., Jolly, W.M., Piper, S.C., Tucker, C.J., Myneni, R.B., Running, S.W., 2003. Climate-driven increases in global terrestrial net primary production from 1982 to 1999. *Science* 300, 1560–1563.
- Nobel, P., Forseth, I., Long, S., 1993. Canopy structure and light interception. In: *Photosynthesis and Production in a Changing Environment: A Field and Laboratory Manual*, pp. 79–90.
- Oquist, G., Huner, N.P.A., 2003. Photosynthesis of overwintering evergreen plants. *Annu. Rev. Plant Biol.* 54, 329–355.
- Pacheco-Labrador, J., Martin, M.P., 2014. Nonlinear response in a field portable spectroradiometer: characterization and effects on output reflectance. *IEEE Trans. Geosci. Remote Sens.* 52, 920–928.
- Parazoo, N.C., Bowman, K., Frankenberg, C., Lee, J.E., Fisher, J.B., Worden, J., Jones, D.B.A., Berry, J., Collatz, G.J., Baker, I.T., Jung, M., Liu, J.J., Osterman, G., O'Dell, C., Sparks, A., Butz, A., Guerlet, S., Yoshida, Y., Chen, H.L., Gerbig, C., 2013. Interpreting seasonal changes in the carbon balance of southern Amazonia using measurements of XCO₂ and chlorophyll fluorescence from GOSAT. *Geophys. Res. Lett.* 40, 2829–2833.
- Parazoo, N.C., Bowman, K., Fisher, J.B., Frankenberg, C., Jones, D.B., Cescatti, A., Perez-Priego, O., Wohlfahrt, G., Montagnani, L., 2014. Terrestrial gross primary production inferred from satellite fluorescence and vegetation models. *Glob. Chang. Biol.* 20, 3103–3121.
- Pathre, U., Sinha, A.K., Shirke, P.A., Sane, P.V., 1998. Factors determining the midday depression of photosynthesis in trees under monsoon climate. *Trees* 12, 472–481.
- Paul-Limoges, E., Black, T.A., Christen, A., Nesic, Z., Jassal, R.S., 2015. Effect of clearcut harvesting on the carbon balance of a Douglas-fir forest. *Agric. For. Meteorol.* 203, 30–42.
- Paul-Limoges, E., Wolf, S., Eugster, W., Hörtnergl, L., Buchmann, N., 2017. Below-canopy contributions to ecosystem CO₂ fluxes in a temperate mixed forest in Switzerland. *Agric. For. Meteorol.* 247, 582–596.
- Peguero-Pina, J.J., Morales, F., Flexas, J., Gil-Pelegrín, E., Moya, I., 2008. Photochemistry, remotely sensed physiological reflectance index and de-epoxidation state of the xanthophyll cycle in *Quercus coccifera* under intense drought. *Oecologia* 156, 1.
- Pons, T.L., Welschen, R.A., 2003. Midday depression of net photosynthesis in the tropical rainforest tree *Eperua grandiflora*: contributions of stomatal and internal conductances, respiration and Rubisco functioning. *Tree Physiol.* 23, 937–948.
- Porcar-Castell, A., Tyystjärvi, E., Atherton, J., van der Tol, C., Flexas, J., Pfundel, E.E., Moreno, J., Frankenberg, C., Berry, J.A., 2014. Linking chlorophyll *a* fluorescence to photosynthesis for remote sensing applications: mechanisms and challenges. *J. Exp. Bot.* 4065–4095.
- Rascher, U., Nedbal, L., 2006. Dynamics of photosynthesis in fluctuating light - commentary. *Curr. Opin. Plant Biol.* 9, 671–678.
- Rascher, U., Agati, G., Alonso, L., Cecchi, G., Champagne, S., Colombo, R., Damm, A., Daumard, F., de Miguel, E., Fernandez, G., Franch, B., Franke, J., Gerbig, C., Gioli, B., Gómez, J.A., Goulas, Y., Guanter, L., Gutiérrez-de-la-Cámarra, Ó., Hamdi, K., Hostert, P., Jiménez, M., Kosavcova, M., Lognoli, D., Meroni, M., Miglietta, F., Moersch, A., Moreno, J., Moya, I., Neininger, B., Okujeni, A., Ounis, A., Palombi, L., Raimondi, V., Schickling, A., Sobrino, J.A., Stellmes, M., Toci, G., Toscano, P., Udelhoven, T., van der Linden, S., Zaldei, A., 2009. CEFLES2: the remote sensing component to quantify photosynthetic efficiency from the leaf to the region by measuring sun-induced fluorescence in the oxygen absorption bands. *Biogeosciences* 6, 1181–1198.
- Raschke, K., Resemann, A., 1986. The midday depression of CO₂ assimilation in leaves of *Arbutus unedo* L.: diurnal changes in photosynthetic capacity related to changes in temperature and humidity. *Planta* 168, 546–558.
- Ruban, A.V., Young, A.J., Horton, P., 1993. Induction of nonphotochemical energy dissipation and absorbance changes in leaves (evidence for changes in the state of the light-harvesting system of photosystem II in vivo). *Plant Physiol.* 102, 741–750.
- Sanders, A.F.J., Verstraeten, W.W., Kooreman, M.L., van Leth, T.C., Beringer, J., Joiner, J., 2016. Spaceborne sun-induced vegetation fluorescence time series from 2007 to 2015 evaluated with Australian flux tower measurements. *Remote Sens.* 8.
- Schurr, U., Walter, A., Rascher, U., 2006. Functional dynamics of plant growth and photosynthesis - from steady-state to dynamics - from homogeneity to heterogeneity. *Plant Cell Environ.* 29, 340–352.
- Sitch, S., Huntingford, C., Gedney, N., Levy, P., Lomas, M., Piao, S., Betts, R., Caias, P., Cox, P., Friedlingstein, P., 2008. Evaluation of the terrestrial carbon cycle, future plant geography and climate-carbon cycle feedbacks using five Dynamic Global Vegetation Models (DGVMs). *Glob. Chang. Biol.* 14, 2015–2039.
- Špunda, V., Kalina, J., Urban, O., Luis, V., Sibisse, I., Puertolas, J., Šprtová, M., Marek, M., 2005. Diurnal dynamics of photosynthetic parameters of Norway spruce trees cultivated under ambient and elevated CO₂: the reasons of midday depression in CO₂ assimilation. *Plant Sci.* 168, 1371–1381.
- Sun, Y., Frankenberg, C., Wood, J.D., Schimel, D.S., Jung, M., Guanter, L., Drewry, D.T., Verma, M., Porcar-Castell, A., Griffis, T.J., Gu, L., Magney, T.S., Kohler, P., Evans, B., Yuen, K., 2017. OCO-2 advances photosynthesis observation from space via solar-induced chlorophyll fluorescence. *Science* 358.
- Turner, D.P., Urbanski, S., Bremer, D., Wofsy, S.C., Meyers, T., Gower, S.T., Gregory, M., 2003. A cross-biome comparison of daily light use efficiency for gross primary production. *Glob. Chang. Biol.* 9, 383–395.
- Turner, D.P., Ritts, W.D., Cohen, W.B., Maeirsperger, T.K., Gower, S.T., Kirschbaum, A.A., Running, S.W., Zhao, M.S., Wofsy, S.C., Dunn, A.L., Law, B.E., Campbell, J.L., Oechel, W.C., Kwon, H.J., Meyers, T.P., Small, E.E., Kurc, S.A., Gamon, J.A., 2005. Site-level evaluation of satellite-based global terrestrial gross primary production and net primary production monitoring. *Glob. Chang. Biol.* 11, 666–684.
- van der Tol, C., Verhoef, W., Rosema, A., 2009a. A model for chlorophyll fluorescence and photosynthesis at leaf scale. *Agric. For. Meteorol.* 149, 96–105.
- van der Tol, C., Verhoef, W., Timmermans, J., Verhoef, A., Su, Z., 2009b. An integrated model of soil-canopy spectral radiances, photosynthesis, fluorescence, temperature and energy balance. *Biogeosciences* 6, 3109–3129.
- van der Tol, C., Rossini, M., Cogliati, S., Verhoef, W., Colombo, R., Rascher, U., Mohammed, G., 2016. A model and measurement comparison of diurnal cycles of sun-induced chlorophyll fluorescence of crops. *Remote Sens. Environ.* 186, 663–677.
- Verma, M., Schimel, D., Evans, B., Frankenberg, C., Beringer, J., Drewry, D.T., Magney, T., Marang, I., Hutley, L., Moore, C., Eldering, A., 2017. Effect of environmental conditions on the relationship between solar-induced fluorescence and gross primary productivity at an OzFlux grassland site. *J. Geophys. Res. Biogeosci.* 122, 716–733.
- Verrelst, J., Schaepman, M.E., Koetz, B., Kneubühler, M., 2008. Angular sensitivity analysis of vegetation indices derived from CHRIS/PROBA data. *Remote Sens. Environ.* 112, 2341–2353.
- Verrelst, J., Rivera, J.P., van der Tol, C., Magnani, F., Mohammed, G., Moreno, J., 2015. Global sensitivity analysis of the SCOPE model: what drives simulated canopy-leaving sun-induced fluorescence? *Remote Sens. Environ.* 166, 8–21.
- Vickers, D., Mahrt, L., 1997. Quality control and flux sampling problems for tower and aircraft data. *J. Atmos. Ocean. Technol.* 14, 512–526.
- Villar, R., Held, A.A., Merino, J., 1995. Dark leaf respiration in light and darkness of an evergreen and a deciduous plant species. *Plant Physiol.* 107, 421–427.
- Walther, S., Voigt, M., Thum, T., Gonsamo, A., Zhang, Y., Köhler, P., Jung, M., Varlagin, A., Guanter, L., 2016. Satellite chlorophyll fluorescence measurements reveal large-scale decoupling of photosynthesis and greenness dynamics in boreal evergreen forests. *Glob. Chang. Biol.* 22, 2979–2996.
- Williams, M., Rastetter, E.B., Fernandes, D.N., Goulden, M.L., Wofsy, S.C., Shaver, G.R., Melillo, J.M., Munger, J.W., Fan, S.M., Nadelhoffer, K.J., 1996. Modelling the soil-plant-atmosphere continuum in a *Quercus-Acer* stand at Harvard Forest: the regulation of stomatal conductance by light, nitrogen and soil/plant hydraulic properties. *Plant Cell Environ.* 19, 911–927.
- Wood, J.D., Griffis, T.J., Baker, J.M., Frankenberg, C., Verma, M., Yuen, K., 2017. Multiscale analyses of solar-induced fluorescence and gross primary production. *Geophys. Res. Lett.* 44, 533–541.
- Xu, D.-Q., Shen, Y.-K., 2005. External and internal factors responsible for midday depression of photosynthesis. In: *Handbook of Photosynthesis*, Second edition. CRC Press.
- Zarco-Tejada, P.J., Morales, A., Testi, L., Villalobos, F.J., 2013. Spatio-temporal patterns of chlorophyll fluorescence and physiological and structural indices acquired from hyperspectral imagery as compared with carbon fluxes measured with eddy covariance. *Remote Sens. Environ.* 133, 102–115.
- Zhang, S., Gao, R., 2000. Diurnal changes of gas exchange, chlorophyll fluorescence, and stomatal aperture of hybrid poplar clones subjected to midday light stress. *Photosynthetica* 37, 559–571.